Test Report

Cold Performance Tests on FM High Stress Ge:Ga Detector Modules

L. Barl

10.08.2006

	Name	*Function*	*Date*	*Signature*
Prepared by	L. Barl			
Approved by	A. Poglitsch			
Approved by	R. Katterloher			

Contents

1 Scope

This report shows the results of 10 test runs on the high stress PACS FM Ge:Ga-detector modules carried out at the MPE between January and April 2006. Altogether, 31 modules have been tested. Some modules were tested 3 times because of exchange of defect CREs or repair of suspicious detector pixels (open, strong, weak and spiking pixels).
Improvements of the test setup with respect to the measurements on QM modules delivered much more reliable responsivity values (new cryogenic BB without any filters) and lower noise, because of the implementation of additional sense wires for the sensitive supply lines of the CRE.

The responsivity measurements on the modules are considered as key inspection points. Based on the results of these cryogenic performance tests, 25 modules were selected for the integration of the high stress detector array in the PACS flight model.

Between the 2 test runs of Sevenpack HS 1 the modules were 10 times cryo-cycled at 4K, 1 defect CRE was exchanged against a new one and open pixels were re-glued. The comparison of the results of both tests should identify the influence of multiple cool downs on the performance of the detectors modules equipped with new designed FM CREs .

2 Related Documents

PACS-ME-DS-002
PACS-ME-TR-016
PACS-ME-TR-062
PACS-ME-TR-064
PACS-ME-TR-065
PACS-MA-TR-014

3 Test Samples

The following high stress modules, integrated in several 'FM Sevenpacks' were tested:

FM HS 1: FM153, FM158, FM159, FM160, FM161, FM165, FM168
FM HS 1c: FM158, FM159, FM162, FM171, FM173, FM174
FM HS 2b: FM172, FM177, FM183, FM184, FM186
FM HS 3: FM169, FM170, FM175, FM176, FM179, FM180, FM181
FM HS 4: FM153, FM160, FM164, FM187, FM188, FM189, FM190
FM HS 5: FM159, FM161, FM162, FM168, FM180, FM186, FM187
FM HS 6: FM169, FM171, FM181, FM189
FM HS 10: FM192, FM196
FM HS 11: FM191, FM195

	HS 1(1)	HS 1(2)	HS 1c	HS 2b	HS 3	HS 4	HS 5	HS 6	HS10	HS 11
FM153	x	x				X (new FEE)				
FM158	x	X (new FEE)	x							
FM159	x	x	x				X (new FEE)			
FM160	x	x				X (new FEE)				
FM161	x	x					x			
FM162			x				x			
FM164						x				
FM165	x	x								
FM168	x	x					x			
FM169					x			X (new FEE)		
FM170					x					
FM171			x					X (new FEE)		
FM172				x						
FM173			x							
FM174			x							
FM175					x					
FM176					x					
FM177				x						
FM179					x					
FM180					x		x			
FM181					x			X (new FEE)		
FM183				x						
FM184				x						
FM186				x			X (new FEE)			
FM187						x	X (new FEE)			
FM188						x				
FM189						x		X (new FEE)		
FM190						x				
FM192									x	
FM196									x	
FM191										x
FM195										x

Table 1 shows the test matrix of all modules, red marked crosses indicate defect FEEs at the 1st test run with no output frames, which were replaced. The other new FEEs were integrated after measuring higher or lower currents in at least one supply line of the original FEE. After the 1st performance test of HS 1(1) the modules were cryo-cycled 10 times and retested (HS 1(2)) to investigate performance changes due to the multiple cryo-cycling. Unfortunately only 4 modules out of 7 can be compared, 3 modules got defect during one of the 2 test runs.

Test housing	Dark current	Resp.	Detector Temp.[K]	Integration Capacities	Bias [mV]	Flux [W/pix]	Remarks
HS 1 (1) (1st test) 6 modules	tint=1s 64 ramps	tint=0.25s 128 ramps	1.7 1.85 2.0	all	0 – 90 Δ_{bias}=10	dark *) $1.0e^{-14}$ $4.0e^{-14}$ $1.1e^{-13}$	5 modules o.k. 2 modules defect high dark currents
HS 1 (2) (2nd test) 5 modules	tint=1s 64 ramps	tint=0.25s 128 ramps tint=1/8... 2s 128 ramps	1.85	all	0 – 90 Δ_{bias}=10	dark $4.0e^{-15}$ $1.0e^{-14}$ $4.0e^{-14}$ $1.1e^{-13}$	5 modules o.k. 2 modules defect “normal” dark currents
HS 3 7 modules	tint=1s 64 ramps	tint=0.25s 128 ramps	1.85	all	0 – 90 Δ_{bias}=10	dark $4.0e^{-15}$ $1.0e^{-14}$ $4.0e^{-14}$ $1.1e^{-13}$	all modules o.k.
HS 1c 6 modules	tint=1s 64 ramps	tint=0.25s 128 ramps tint=1/8... 4s 1024..32 ramps	1.85	all	0 – 90 Δ_{bias}=10	dark $4.0e^{-15}$ $1.0e^{-14}$ $4.0e^{-14}$ $1.1e^{-13}$	all modules o.k.
HS 2b 5 modules	tint=1s 64 ramps	tint=0.25s 128 ramps	1.85	all	0 – 90 Δ_{bias}=10	dark $2.4e^{-15}$ $4.0e^{-15}$ $1.0e^{-14}$ $4.0e^{-14}$ $1.1e^{-13}$	all modules o.k.
HS 4 6 modules	tint=1s 64 ramps	tint=0.25s 128 ramps	1.85	all	0 – 90 Δ_{bias}=10	dark $2.4e^{-15}$ $4.0e^{-15}$ $1.0e^{-14}$ $4.0e^{-14}$	all modules o.k.
HS 5 7 modules	tint=1s 64 ramps	tint=0.25s 128 ramps	1.85	all	0 – 90 Δ_{bias}=10	dark $2.4e^{-15}$ $4.0e^{-15}$ $1.0e^{-14}$ $4.0e^{-14}$ $1.1e^{-13}$	all modules o.k.
HS 6 5 modules	tint=1s 64 ramps	tint=0.25s 128 ramps	1.85	all	0 – 90 Δ_{bias}=10	dark $2.4e^{-15}$ $4.0e^{-15}$	4 modules o.k. 1 module defect
HS10 **HS11** 2 modules each	tint=1s 64 ramps	tint=0.25s 128 ramps tint=1/8... 4s 1024..32 ramps	1.85	all	0 – 90 Δ_{bias}=10	dark $2.4e^{-15}$ $4.0e^{-15}$ $1.0e^{-14}$ $4.0e^{-14}$	3 modules ok 1 module of HS11 defect at 4K

Table 2: Measurement settings of all test runs
*) see chapter 5.2

Table 2 lists the standard measurement settings used for all test runs. During all measurements the dummy resistor was not biased. A few additional measurements were done with the Sevenpack FM_sev1 and FM_sev1c to investigate the influence of the integration time on the signal (e.g. de-biasing, linearity) .
Because of the tight test schedule the dependence of the detector performance from the detector temperature was only measured during the first test run of HS 1. All other tests were carried out at the nominal temperature of T=1.85K.
The settings for the responsivity measurements were normally 128 ramps with 0.25s integration time, while for the dark current measurements 64 ramps with 1s integration time were selected. For the integration capacities the values determined by MPIA were used (140, 230, 430 and 1090pF).
Before each cold performance test, each detector module was tested at room temperature by monitoring the supply currents (not all supply lines) and observing the output frames.

4 Test Setup

4.1 Improvements of the Electrical Setup

The mechanical, optical and electrical set-up is described in the doc. PACS-ME-TR-016. Further improvements were made by installing 10 filter capacitors at the connector distribution panel inside the cryostat. This capacitors buffer the most sensitive supply lines against their reference signals and are of the same type as to the capacitors on the distribution board inside the FPU (WIMA MKS 6,8µF).

A second improvement was achieved by using sense lines for the VDDA, VSS ,GND, VDDr and Zero_bias supply lines, which resulted in a better noise performance of the electrical set-up.

4.2 New Test Optics Without Filters

The new cryogenic test optics includes only a black body, 1 mirror, but no attenuation filters. The temperature of the BB, which has the same design as the BBs in the PACS test optics, can be regulated between 4.2 K and 300 K. For the presented data the BB temperature was adjusted between 8.5K and 14K, which results in a flux change by a factor ~50. The stability of the BB is better than 1mK, a calibrated Ge temperature sensor is used as input for the temperature controller.

With this filter free set-up we get rid of all the known problems, like uncertainty of cold transmission curves and filter temperature, multiple reflections between filter stacks, which can make flux calculations more difficult.

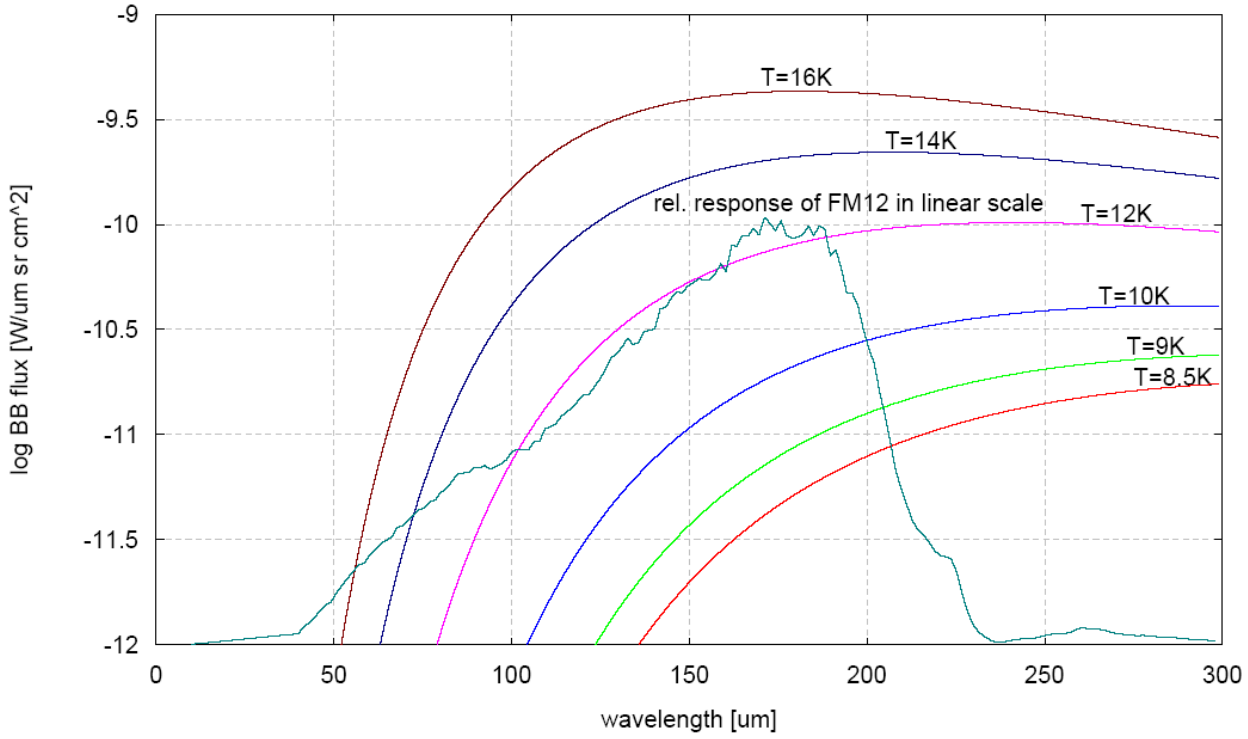

Fig. 1: Planck function for different black body temperatures

Fig. 1 shows the spectral flux distribution for a BB with temperature settings between 8.5K and 16K. The curve of the relative response (in arbitrary units) of a detector from FM12 should show how the black body flux distribution covers the detector response. The flux was calculated by integration over the product of spectral BB radiation intensity, a geometric factor and the relative detector response, which was normalized to 1 at the peak wavelength. The result of this calculation gives an equivalent flux at the peak wavelength of the detector.

$$F_{BB}(T) = \int 2\,\frac{h \cdot c^2}{\lambda^5}\,\frac{1}{e^{hc/\lambda kT} - 1}\;\cdot A_{det} \cdot \Omega \cdot rel.response(\lambda)\;\cdot\; d\lambda$$

For an accurate flux calculation for each detector pixel one has to use the relative response for each pixel, which was not available (only the first and the last 3 pixel of each module were measured). The different cut-off wavelength of each pixel leads to an error below ±3% of the mean value. For the present report the relative response of one pixel of FM12 was used as reference for all measurements.

All relative response measurements show a small hump between 235 and 300 µm behind the cut-off wavelength. Especially for the flux calculation of the black body at T=8.5K and 9K this feature has an influence on the result. If one calculates the responsivity measured at different black body temperatures, the results indicate that this is an artefact and is not real, because the responsivity at the lower flux levels is also lower. If the hump is not taken into account for the flux calculations, the responsivity becomes more identical for

different BB temperatures

In Table 3, the calculated flux per detector pixel was given for the 6 black body temperatures plotted in Fig.1.

Blackbody temperature [K]	*Flux on HS modules [W/pixel]*
8.5	$2.4\ e^{-15}$
9	$4.0\ e^{-15}$
10	$1.0\ e^{-14}$
12	$4.0\ e^{-14}$
14	$1.1\ e^{-13}$
16	$2.4\ e^{-13}$

Table 3: calculated (peak normalized) mean flux per pixel

5 Results

5.1 Performance change of Sevenpack FM HS 1 due to cryo-cycling

During the first warm functional test (before cryo-cycling) FM158 showed a high current in the VDDD line and no output frames were observed. In the VSS line of FM153 and FM160, a higher current was measured, but normal output frames could be observed. At 4K these 2 modules had strange output frames, which disappeared while pumping down the detector temperature below 2K.
The open pixels of FM159 and FM161 can be identified at room temperature. The cracked pixels in module FM165 can not be distinguished from the other pixels, neither in the warm nor at 2K.

After the cryo cycling, both modules (FM153 and FM160) with the suspicious behavior at 4K during the first test run showed high currents in some supply lines during the warm functional test. While FM153 delivered some output frames, which disturbed the signal of the other connected modules, FM160 was showed no output signal.
FM158 was fully operational after the exchange of the FEE, but pixel 12 was open.
The open pixel (3) in FM159 was re-glued by ASTEQ, but a new open pixel (12) and a 'strong' pixel (16) with a much higher signal was observed after the cycling.
The open pixel in FM161 could not be repaired by ASTEQ, because the damage could not be located in the path from the detectors to the FEE.

The module status of FM HS 1 before and after cryo-cycling is summarized in Table 4, where “open pixel” means no electrical connection between detector and CRE, “weak pixel” means low signal current, most probably due to a high ohmic connection between detector and CRE, and “strong pixel” means high signal current which was not generated by the detector.

Test run	*Module*	*normal pixels*	*open pixels*	*weak pixels*	*strong pixels*	*cracked pixels*	*remarks*
1	FM153	16					~20% higher current in VSS suspicious output frame at 4K -> NCR-ME-NCR-105 / -114
1	FM158						Very high current in VDDD CRE defect, no output frames -> NCR-ME-NCR-103
1	FM159	15	1 (pix3)				o.k.
1	FM160	16					3 times higer current in VSS Suspicious output frame at 4K -> NCR-ME-NCR-104
1	FM161	15	1 (pix10)				o.k.
1	FM165	16				8,10,11,13	o.k.
1	FM168	16					o.k.
2	FM153						Output frames observed, but high currents in VSS and other supply lines -> not connected during test -> NCR-ME-NCR-114
2	FM158	15	1 (pix12)				Repaired, new CRE
2	FM159	15			1(pix16)	pix 12	o.k., pixel 3 reglued
2	FM160						No output frames observed, high currents in some supply lines measured -> not connected during test -> NCR-ME-NCR-113
2	FM161	15	1 (pix10)				o.k.
2	FM165	16				pix 8,10,11,13	o.k.
2	FM168	16					o.k.

Table 4: module status of FM Sevenpack 1 before and after cryo-cycling

The measured “dark” current during the first test was almost 20 times higher compared to the test after the cryo cycling (see Fig.2). This big difference cannot be explained by now. Because the setup was not changed between both test runs, most probably a warm part in the detector test housing was responsible for the high dark current. But the lower values from the 2nd test are still out of spec., which says <50000 e/s.

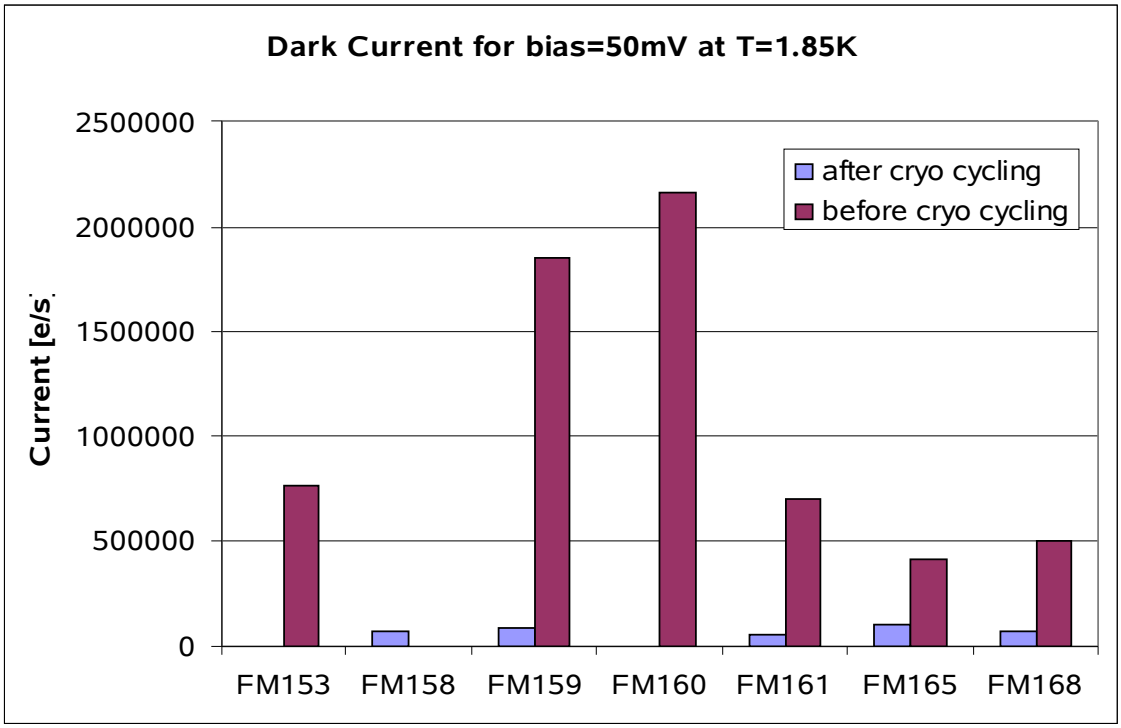

Fig. 2: dark current measured during both test runs

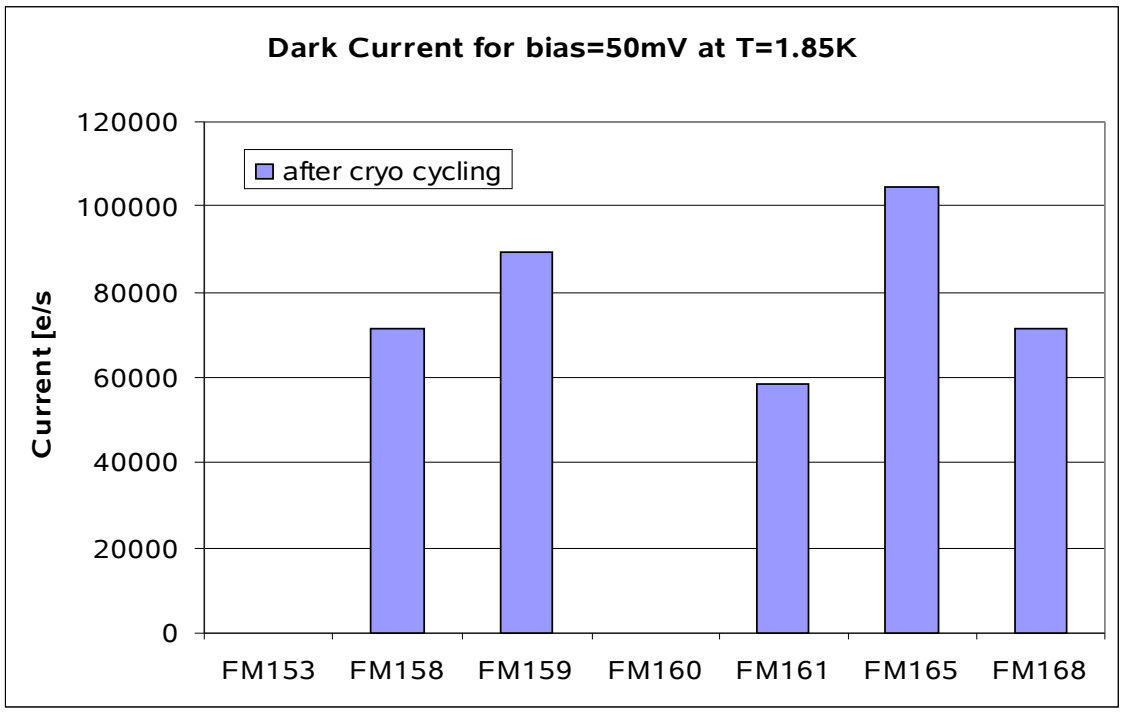

Fig. 3: dark current after cryo cycling

The comparison of Fig. 2 and 3 shows further, that the distribution of the mean values also changed. While during the 1st test, the dark current of FM159 was 4 times higher than of FM165, both modules had similar dark current in the 2nd test. This higher dark current was subtracted for the responsivity calculations.

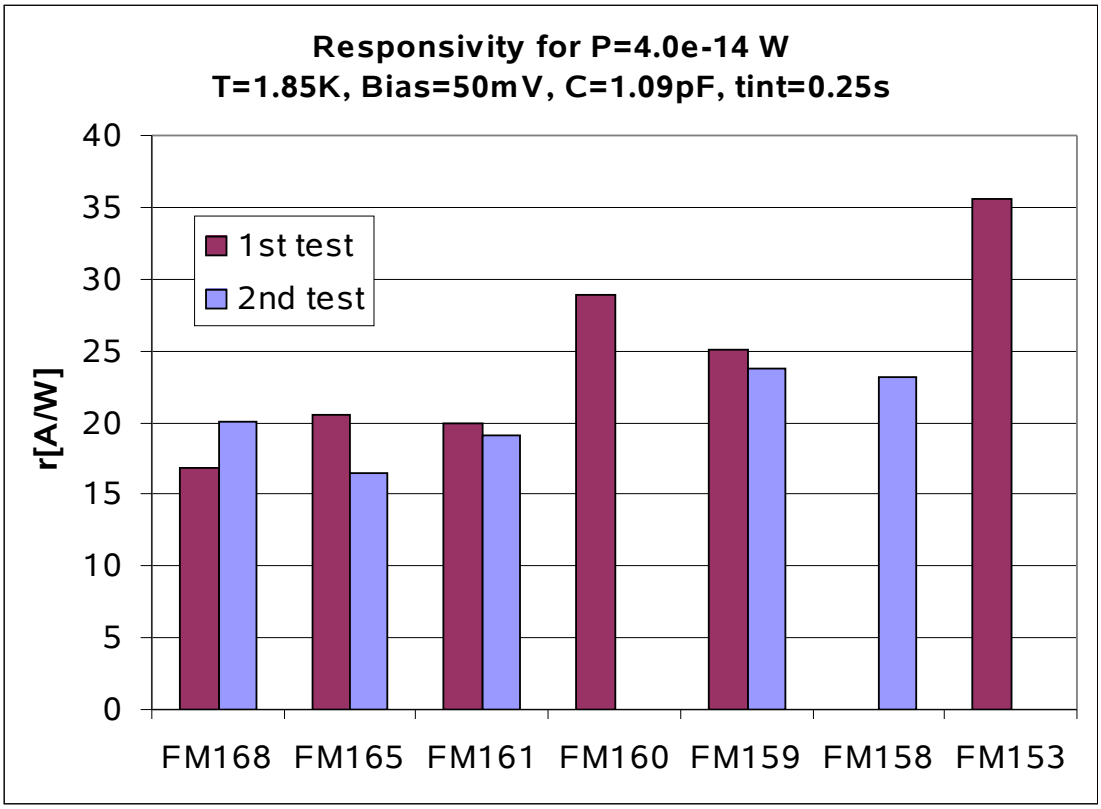

Fig. 4: responsivity measured during both test runs

5.2 Dark current

During the dark current measurements the detectors 'saw' a background of a 4.2K black body, which corresponds to a calculated flux of below $1e^{-18}$ W / pixel as a lower limit, provided there were no light leaks. In the future, a test with 'closed' light cones is planned, to investigate the 'dark' conditions of the setup. If necessary, additional modifications will be made to reach the required low 'dark' background level. The dark current measurement was the first measurement of each test run, before the black body was switched on. This should guarantee that no “warm” parts are present inside the test housing during this very sensitive measurement.

The measured dark current during the first test run with HS 1 is much higher than during all other tests fore unknown reasons.

Fig. 5 shows the dark current of all modules versus bias voltage at T=1.85K. In Fig. 6 . the mean dark current for a bias of 50mV is presented. In both figures, detectors with a very high signal, spiking and open pixels were not considered for the calculations.

The dark current distribution varies by nearly a factor of 3, its value for a bias of 50mV lies between 40000 e^-/s and 135000 e^-/s, which is higher than the specified 50000 e^-/s (red line). A similar distribution was measured for the responsivity (Fig. 25).

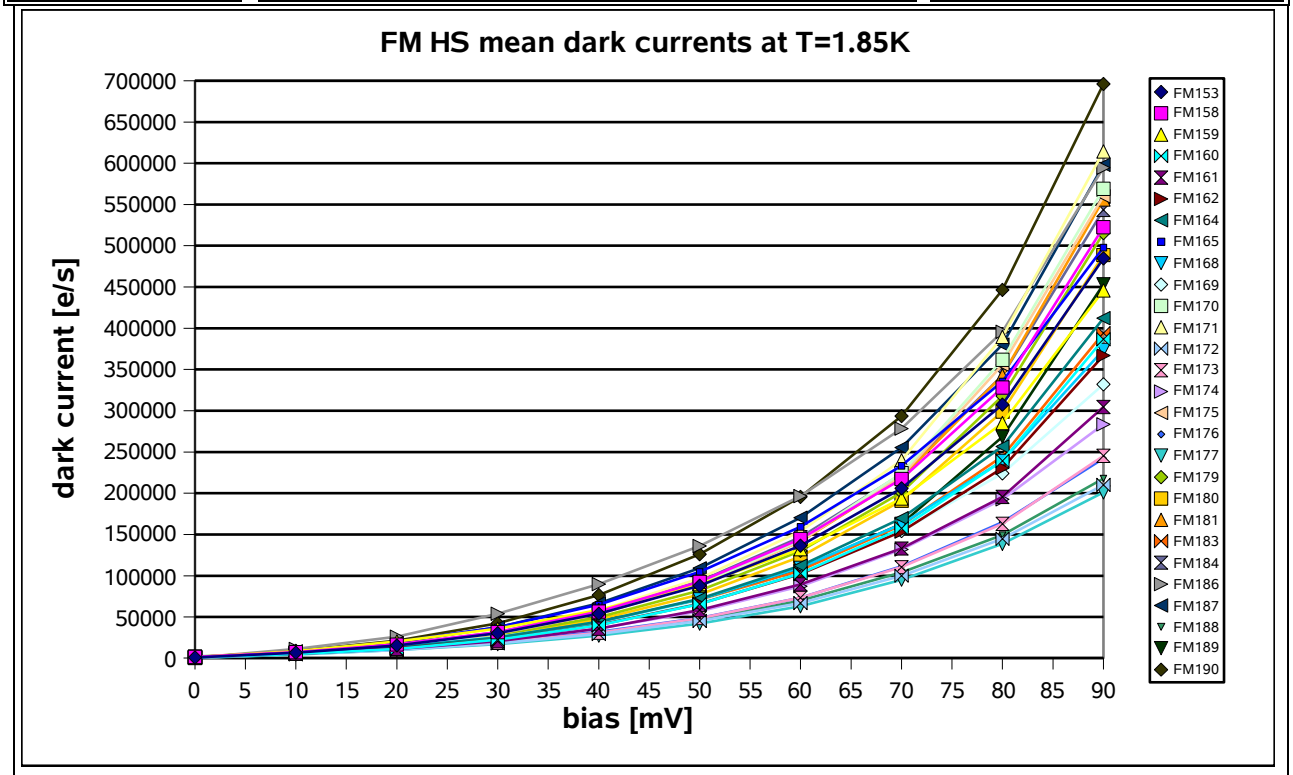

Fig.5 mean dark current of all detector modules versus bias

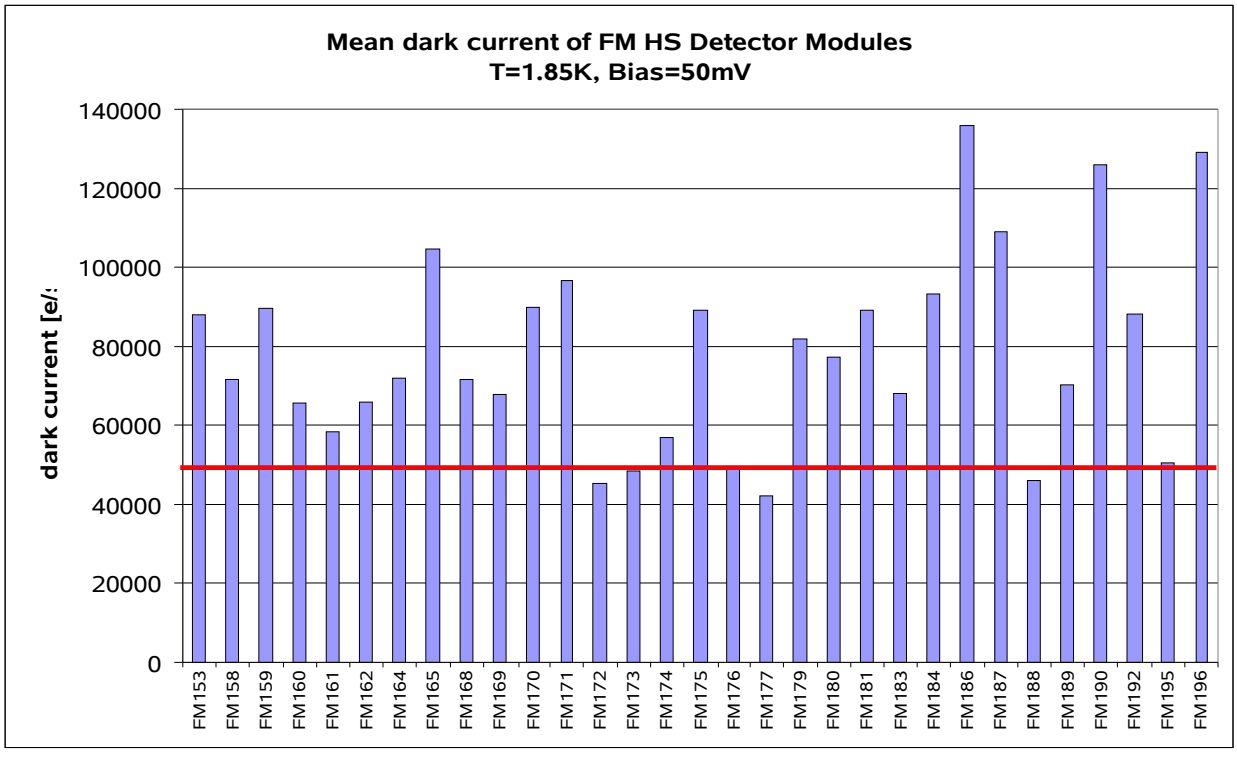

Fig. 6: mean dark current of all modules at T=1.85K and bias=50mV

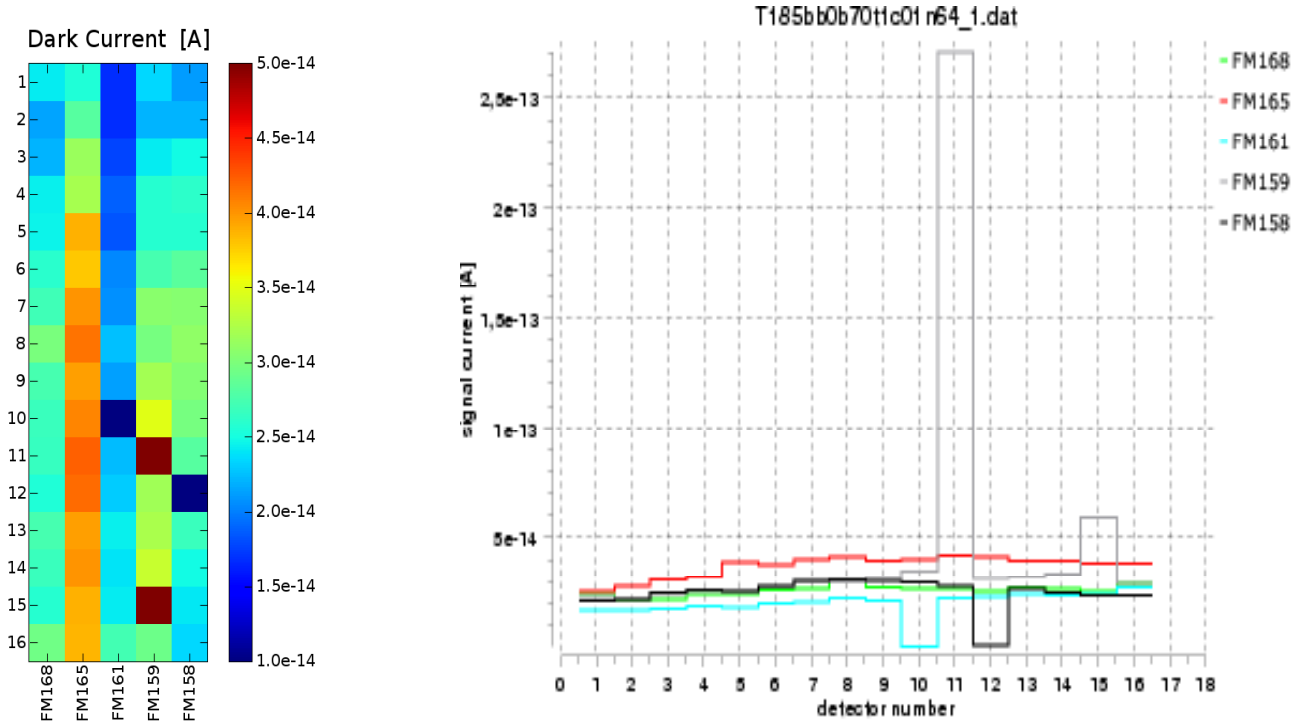

Fig. 7: Dark current of FM HS Sevenpack 1(2) for bias=70mV at T=1.85K

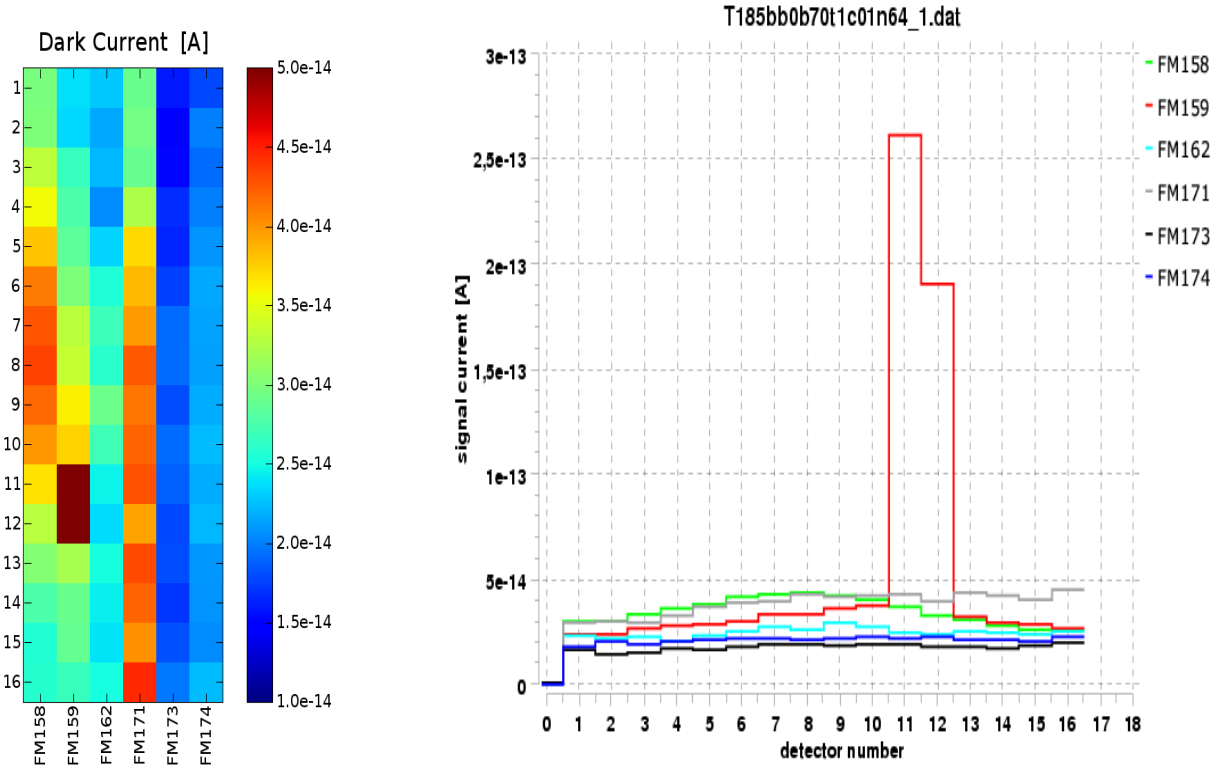

Fig. 8: Dark current of FM HS Sevenpack 1c for bias=70mV at T=1.85K

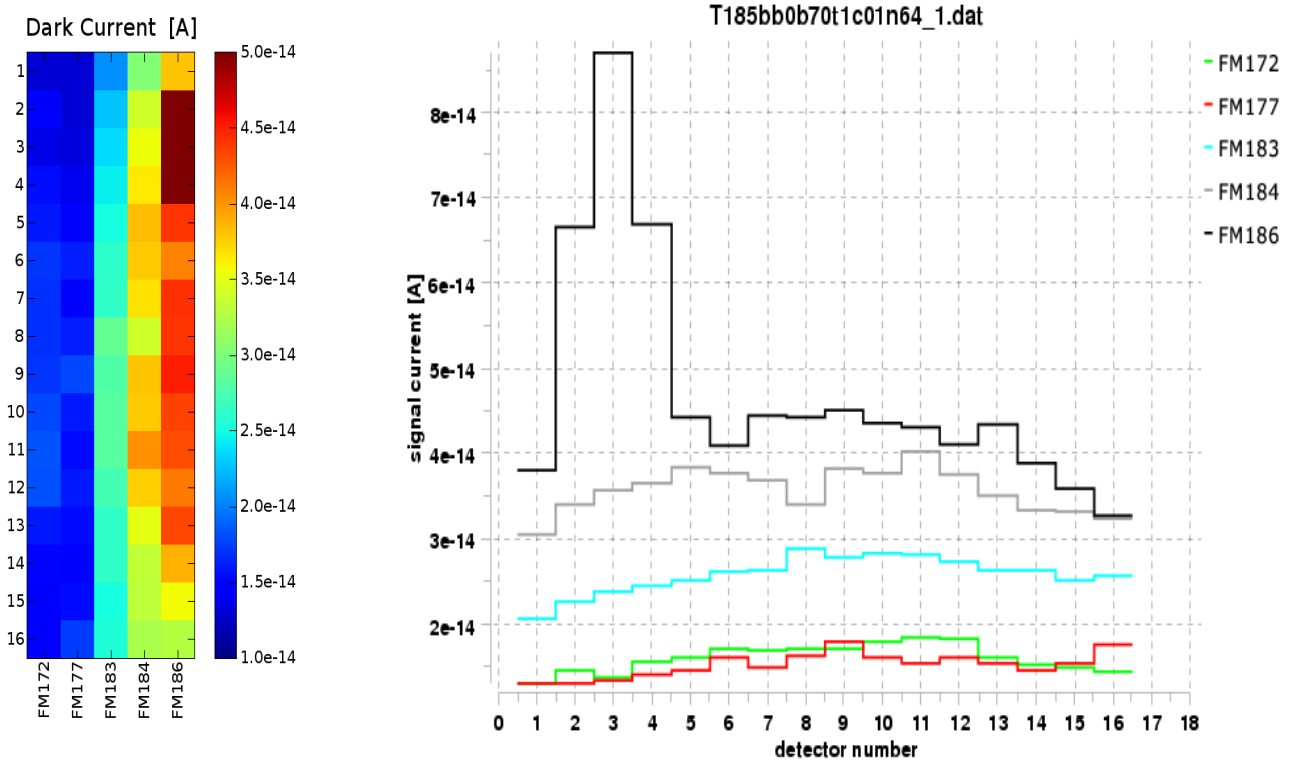

Fig. 9: Dark current of FM HS Sevenpack 2b for bias=70mV at T=1.85K

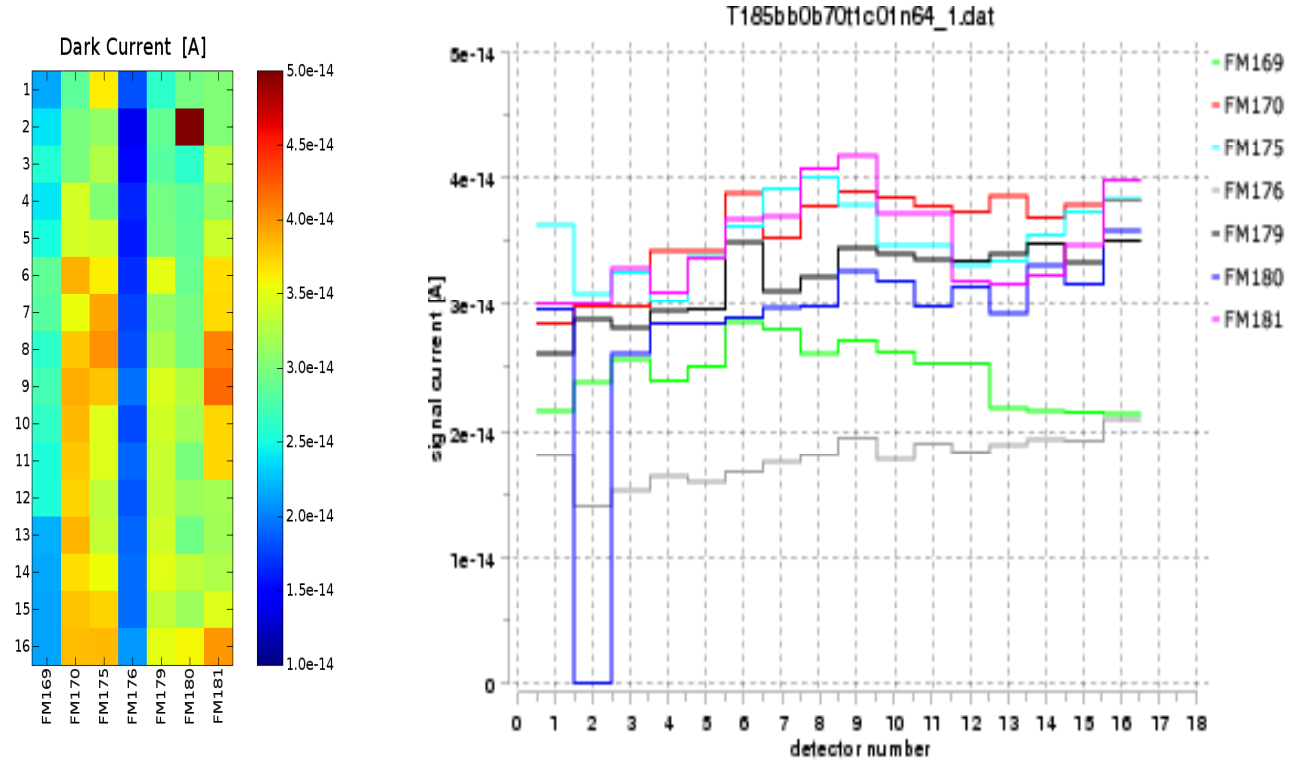

Fig 10: Dark current of FM HS Sevenpack 3 for bias=70mV at T=1.85K

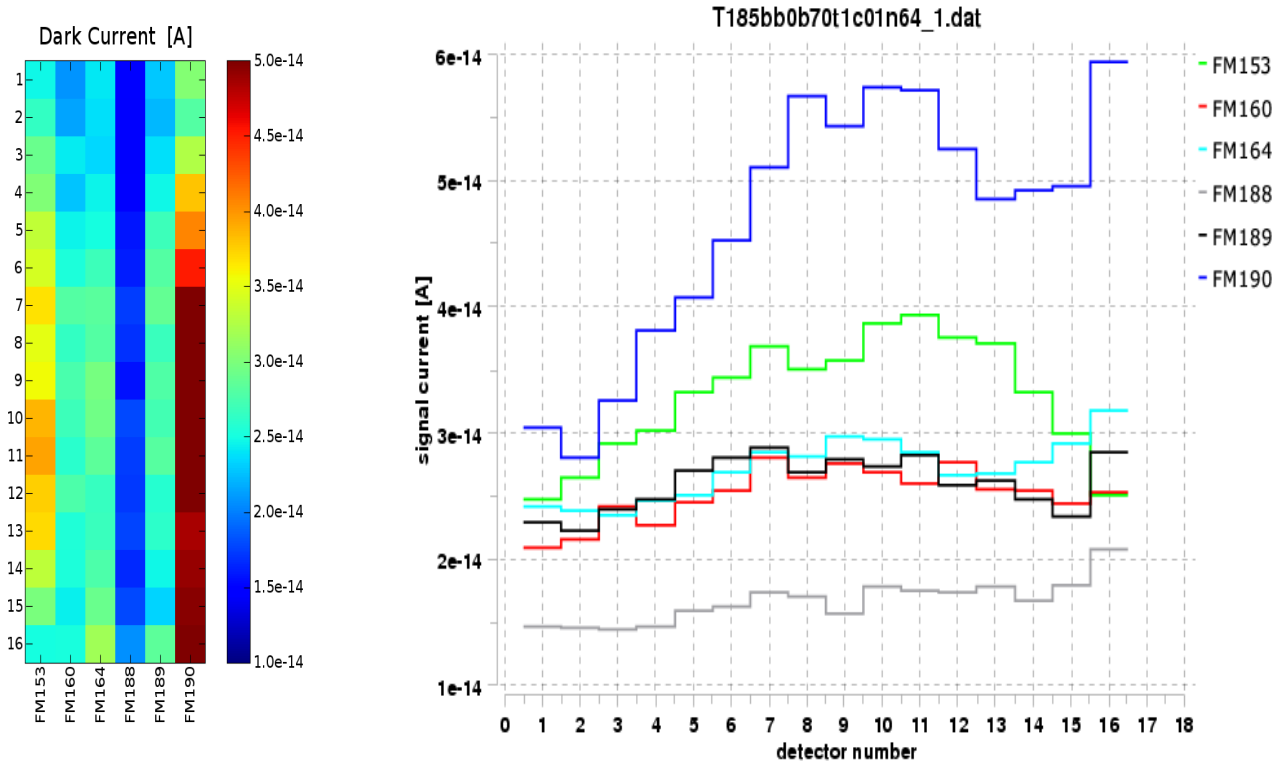

Fig 11: Dark current of FM HS Sevenpack 4 for bias=70mV at T=1.85K

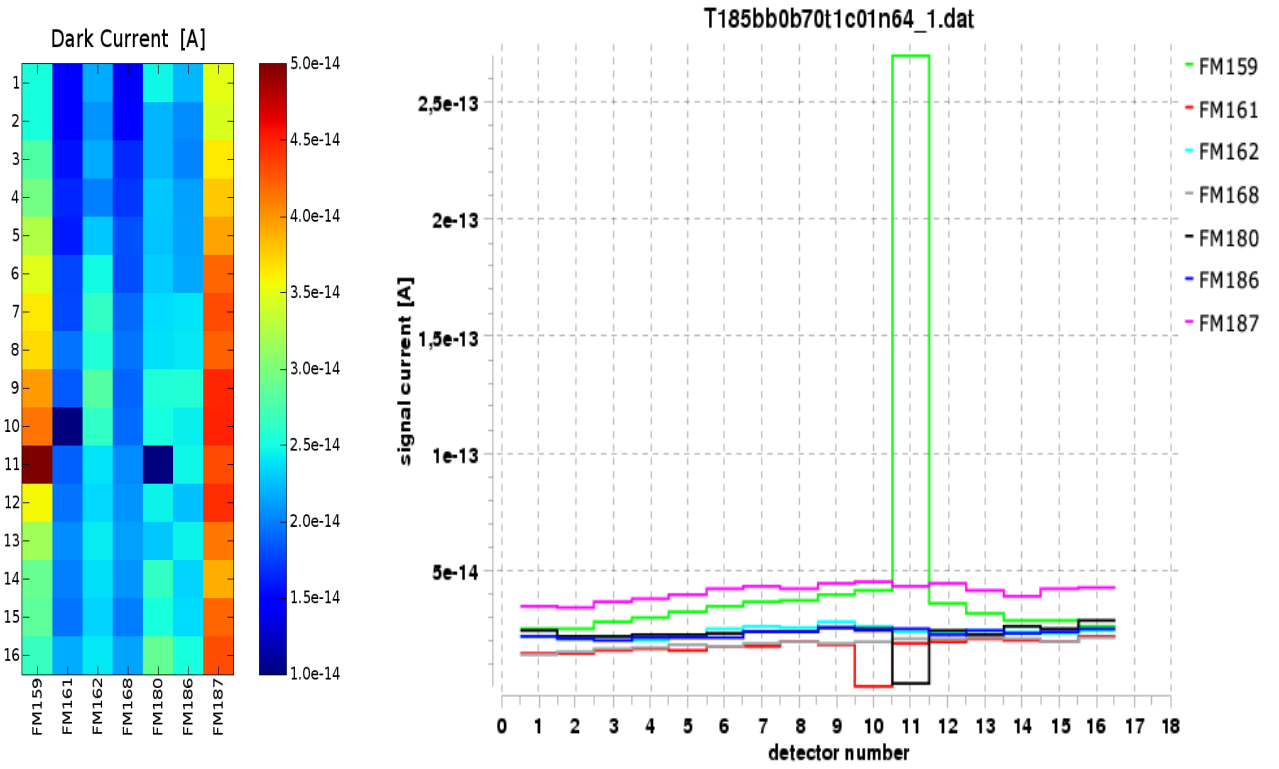

Fig. 12: Dark current of FM HS Sevenpack 5 for bias=70mV at T=1.85K

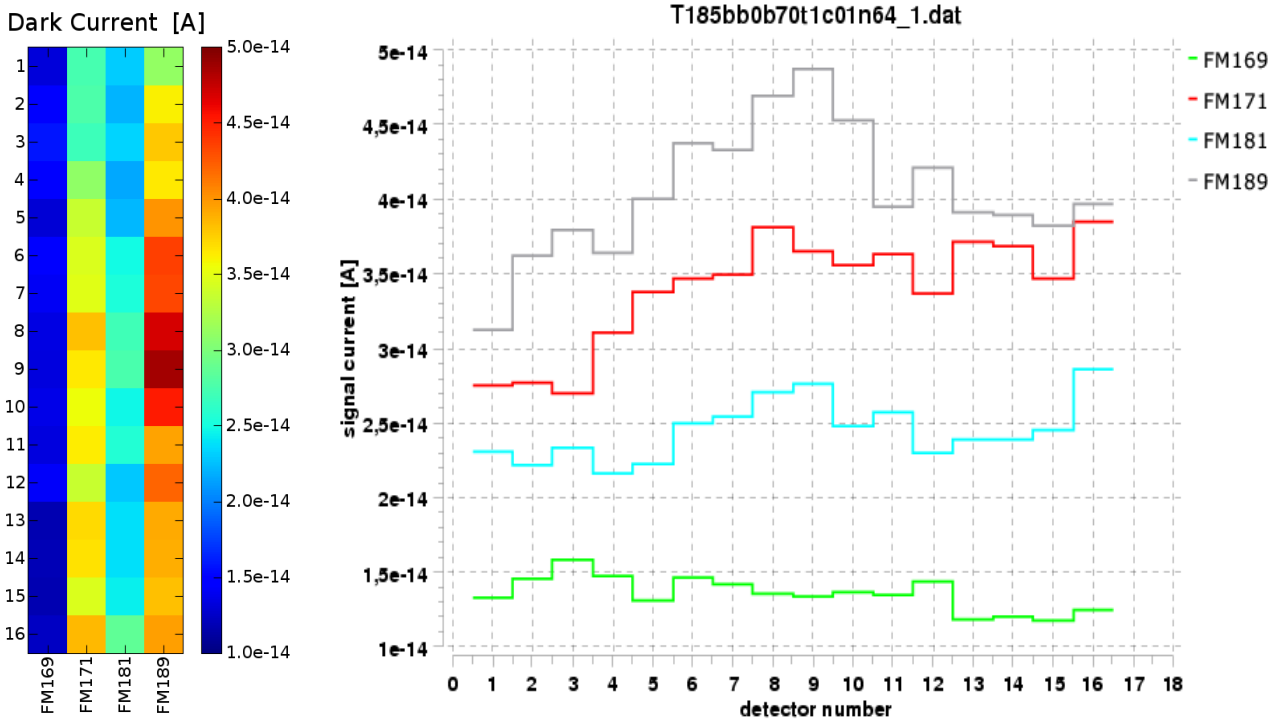

Fig. 13: Dark current of FM HS Sevenpack 6 for bias=70mV at T=1.85K

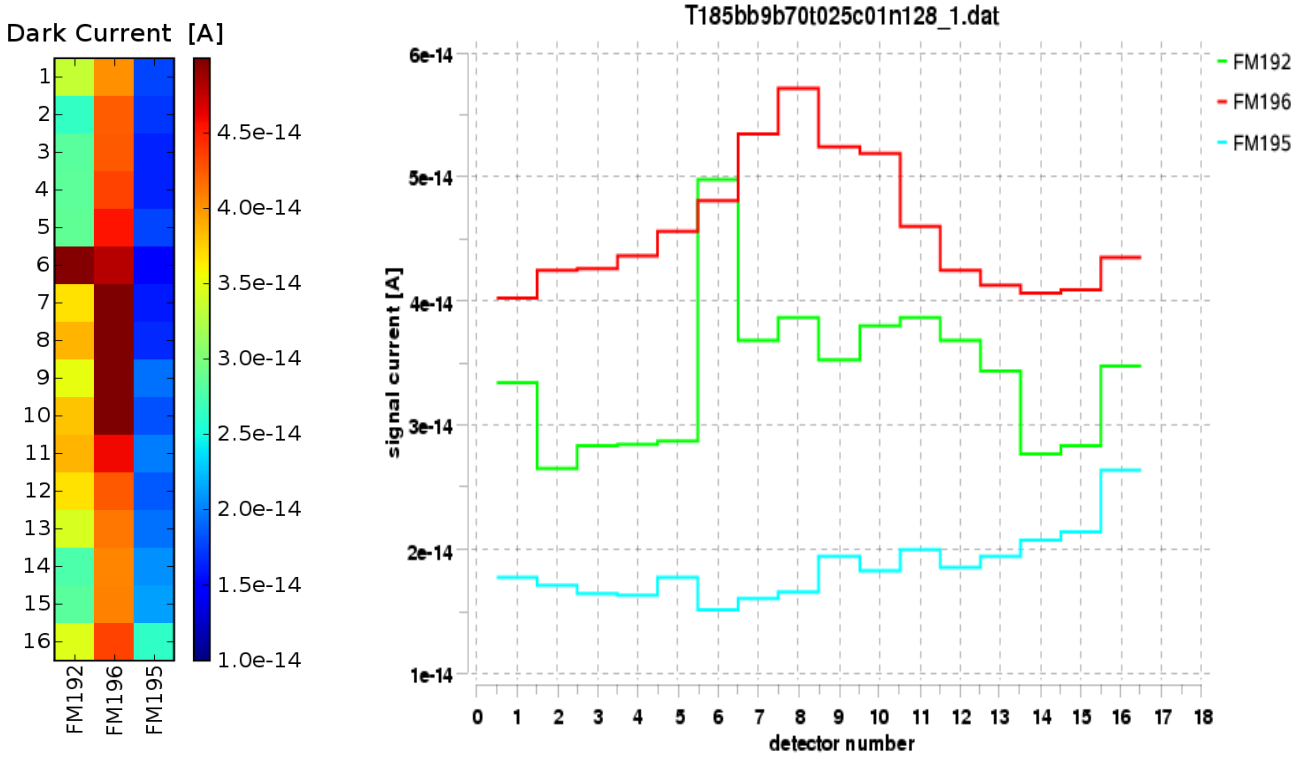

Fig. 14: Dark current of FM HS Sevenpack 10 (FM192 and FM196) and 11 (FM195) for bias=70mV at T=1.85K

Fig. 7 to 14 show the 2-dimensional image of the dark current distribution and the corresponding curve plot for each Sevenpack measured for bias=70mV at T=1.85K. The image plots have a fixed scaling range between 1.0 e^{-14}A and 5.0 e^{-14}A.

Comparing all images one can see that no area of high current is visible, which would indicate a hot spot in the test set-up.

Different behavior was observed of FM159, which was tested 3 times. While in "Sevenpack 1(2)" detector 11 and 16 break through at 70mV, detector 11 and 12 break through in "Sevenpack 1c" and detector 16 behaves normal. During the 3rd test in "Sevenpack 5" only detector 11 broke through, while detector 11 and 16 were normal.

A similar behavior was observed for FM186. In "Sevenpack 2b" detector 3 breaks trough at 70mV bias and the neighbor pixels show strange integration ramps (see Fig. 9). In "Sevenpack 5" all detectors have normal behavior up to 90mV bias.

Open pixels were found in FM161 (pixel 10), FM180 (pixel 2 and 11) and FM158 (pixel 12).

5.3 Responsivity

5.3.1 Temperature dependence of responsivity

The temperature dependence of the responsivity was only measured with HS FM Sevenpack 1 before the cryo cycling. The test was carried out at 3 detector temperatures (1.7K, 1.85K and 2.0K) applying the parameters given in the test matrix (Table 2). Because of the high dark current measured during this test run, it was subtracted from the signal current for responsivity calculation. Between 1.7K and 2.0K the responsivity increases 10% per 0.1K temperature increase. Fig. 15 shows the curves for module FM168, all other modules have a similar behavior.

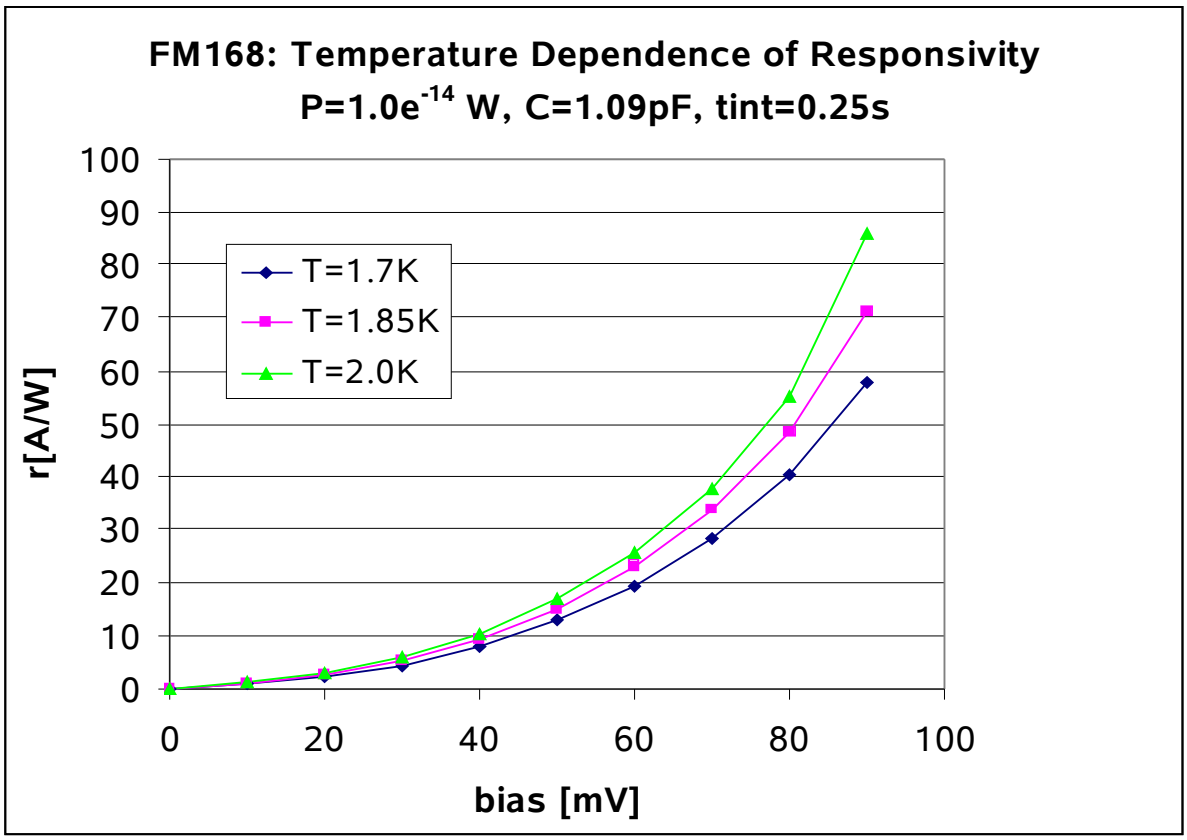

Fig. 15: Temperature dependence of responsivity of FM168 (dark current subtracted)

5.3.2 Detector Responsivity at T=1.85K

A cold black body with different temperatures (8.5K, 9.0K, 10K, 12K, 14K) was used as IR source. The responsivity was calculated for all absolute flux levels ($2.4e^{-15}$W, $4.0e^{-15}$W, $1.0e^{-14}$ W, $4.2e^{-14}$ W and $1.1e^{-13}$ W), considering the dark current impact, which influences the results especially for the low flux levels. Additional curves were plotted, which show the responsivity calculated from the differences of the signal currents and the corresponding flux differences. A typical result is plotted in Fig. 16, where the measured responsivity for 3 absolute flux levels of the black body with T=9K, 10K and 12K and 3 calculated results using flux and signal differences are shown.

The calculated responsivity at a certain bias voltage varies ±10% of the mean value for the selected 6 flux levels. The lower the absolute flux level, the lower the calculated responsivity. The main reason for this effect was the influence of the small hump in the relative response mentioned above. If this hump is not included in the flux calculations, the responsivity becomes higher and therefore fits better the values for the higher flux levels.

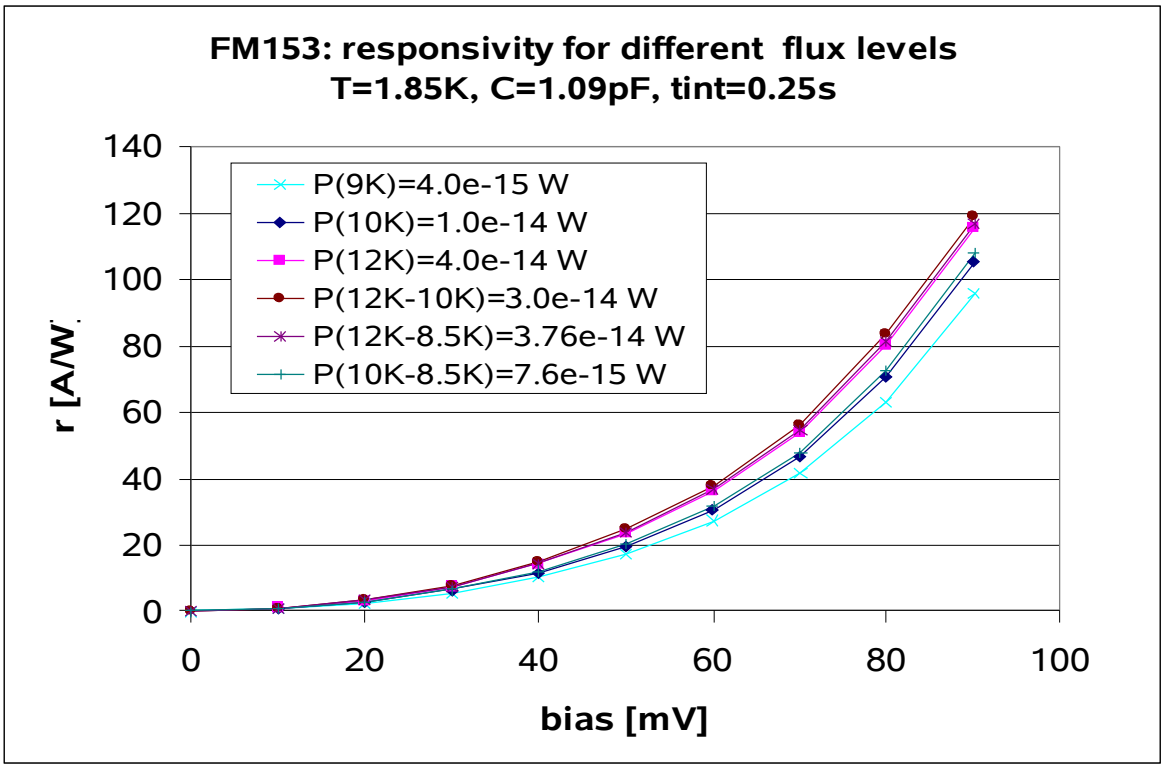

Fig.16: Responsivity of FM153 for different flux levels

On the next pages the images of the responsivity distribution and the corresponding line plot for a bias of 70mV were shown for each Sevenpack. A fixed scaling was used in all plots for easy comparison of all modules. The lower plot on each page indicates the bias dependence of the modules.

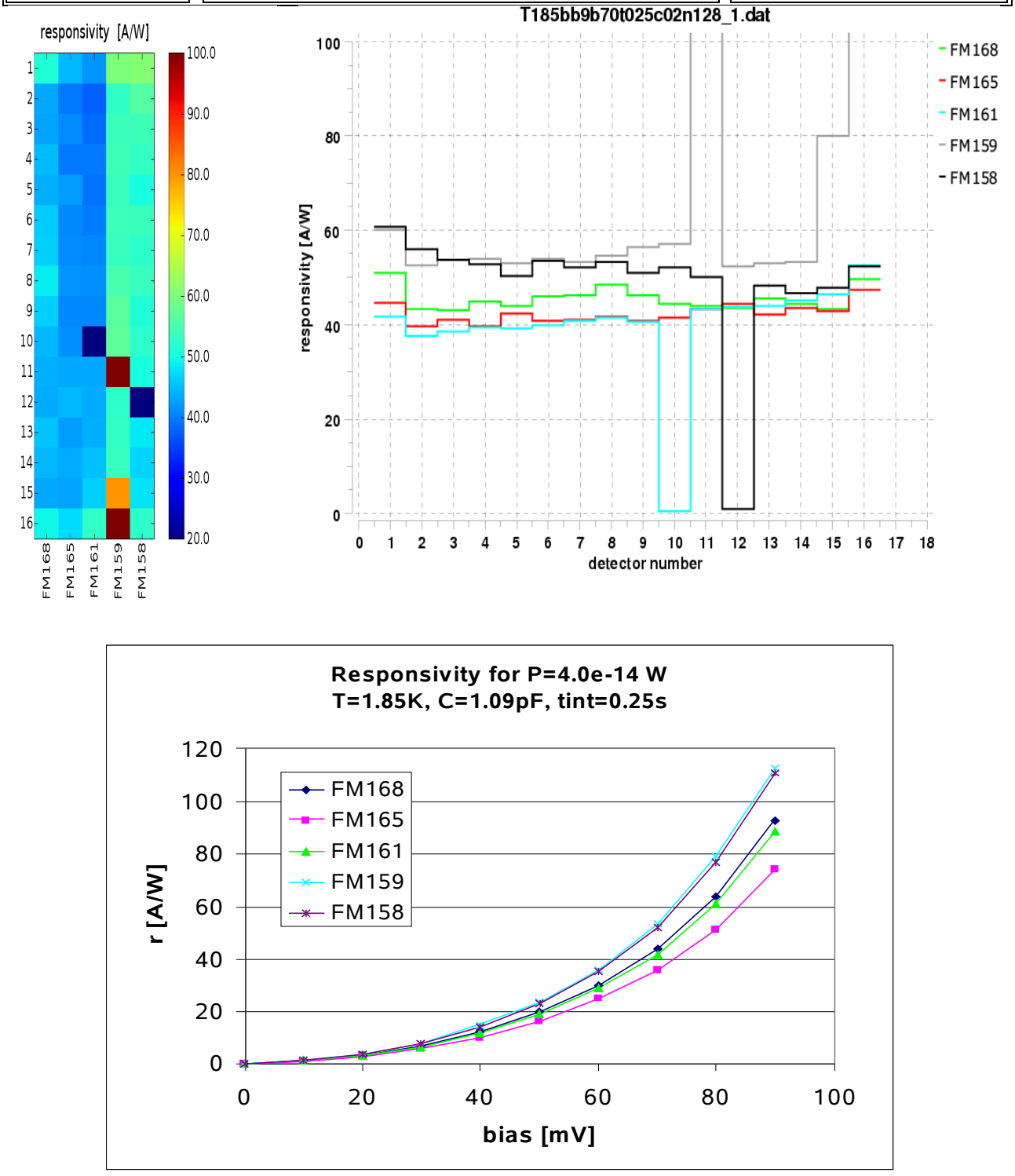

Fig. 17: *FM HS Sevenpack 1(2)*: Open pixel in module FM158 (pix 12) and FM161 (pix 10). In module FM159 pixel 11 break through at bias > 60mV and pixel 16 has a high signal without break trough up to 90 mV. Both pixel show electrical crosstalk to neighbored pixels.

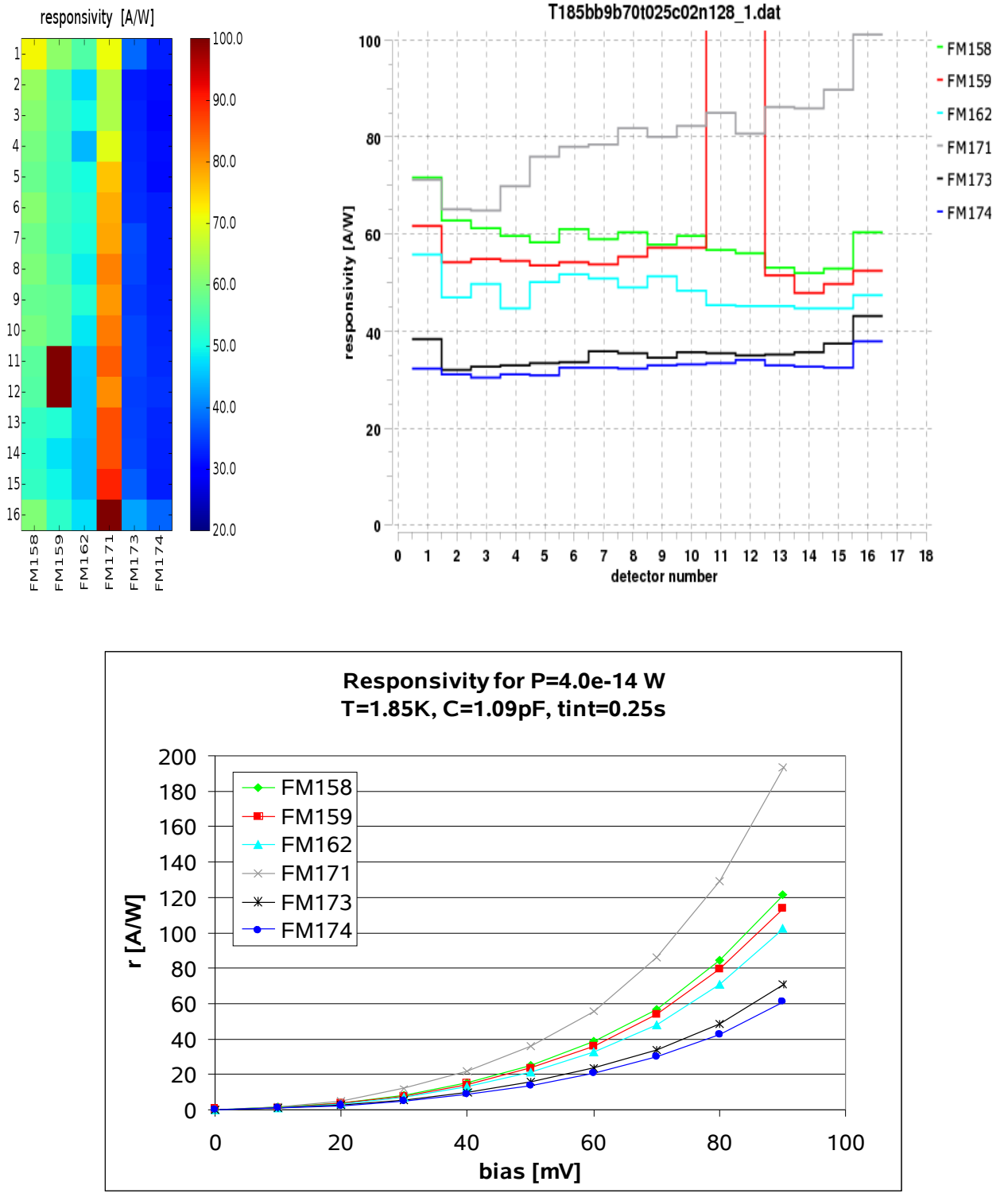

Fig. 18: *FM HS Sevenpack 1c*: Pixel 11 and 12 of FM159 break through for bias > 60mV. Different behavior of pixel 12 and 16 in comparison with FM Sevenpack HS1(2).

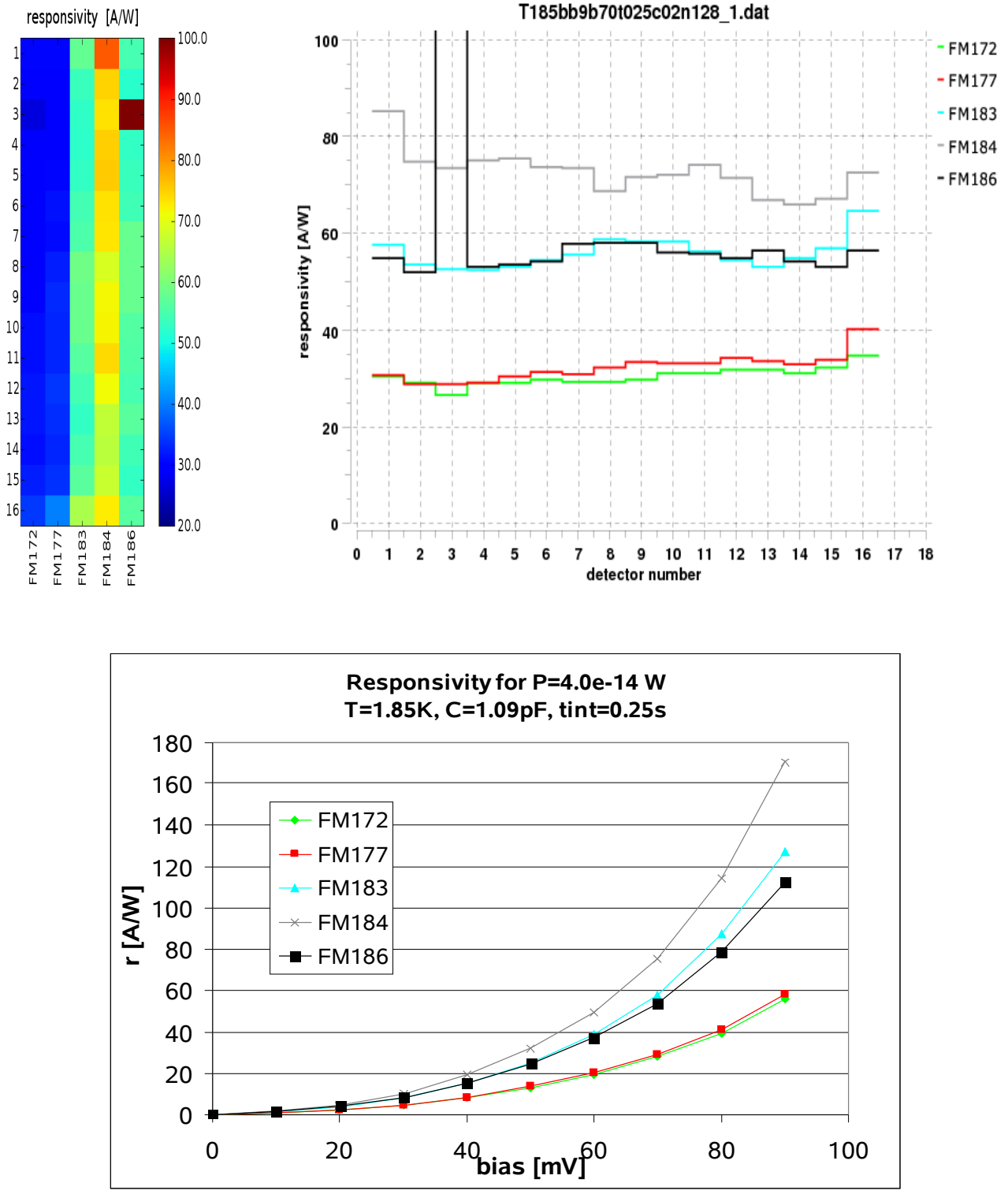

Fig. 19: *FM HS Sevenpack 2b:* Pixel 3 of module FM186 has a very high signal without breakthrough or spiking. The calculated responsivity of this pixel was 700A/W (this cannot be the real responsivity of the detector, but most probably an effect of the FEE/CRE!) for a bias of 70mV.

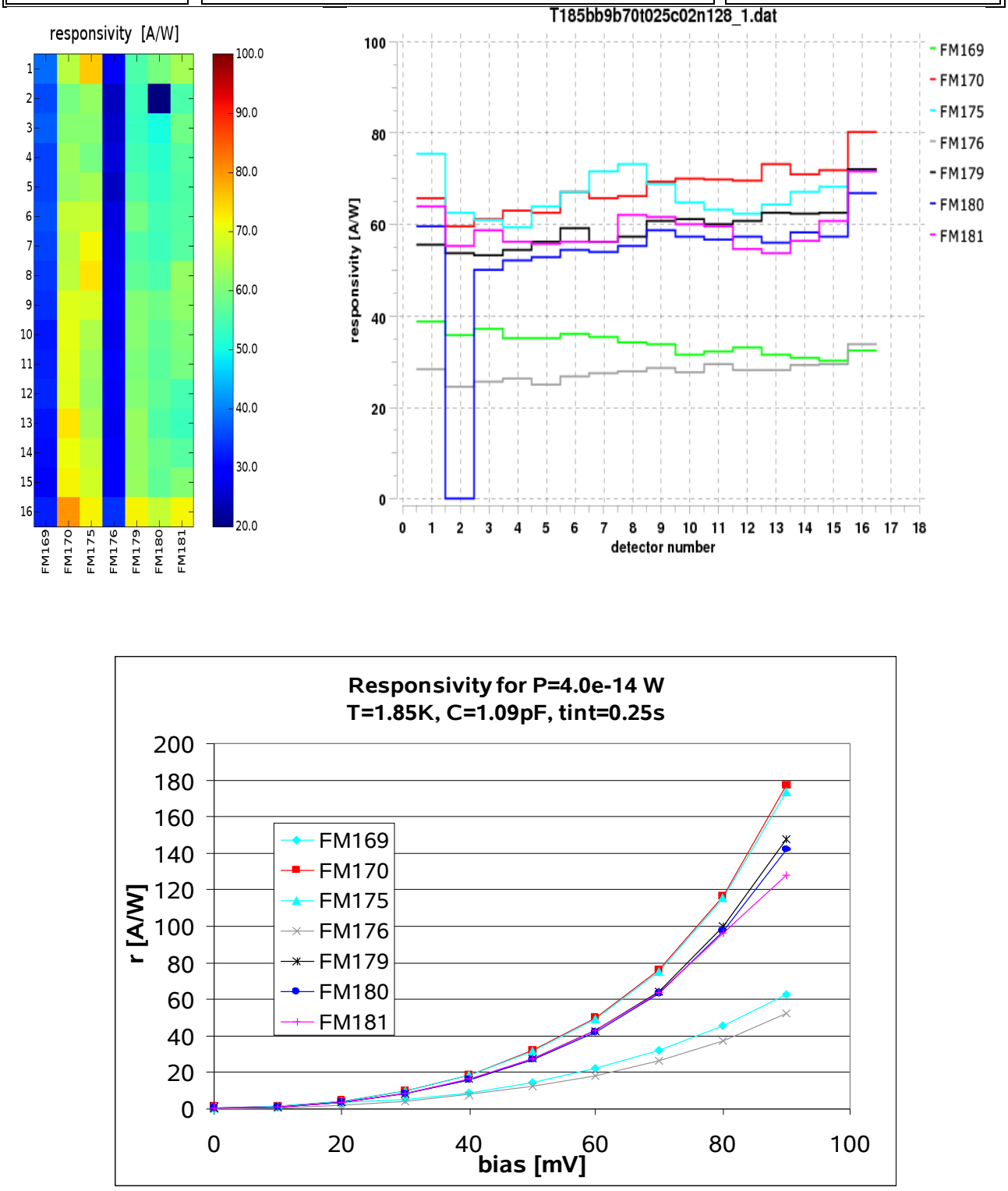

Fig. 20: *FM HS Sevenpack 3*: Pixel 2 open in module FM180

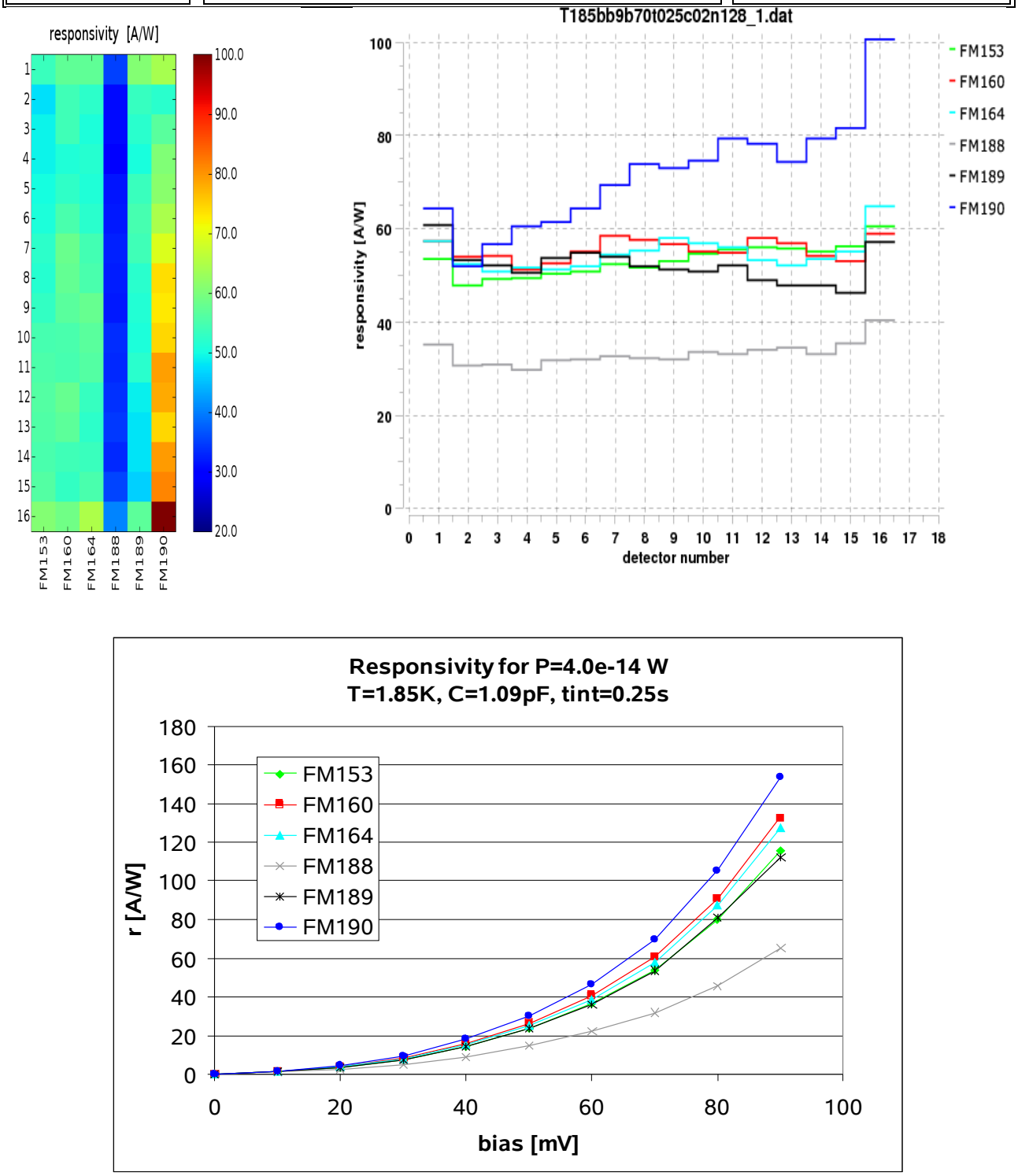

Fig. 21: *FM HS Sevenpack 4:* FM190 very inhomogen

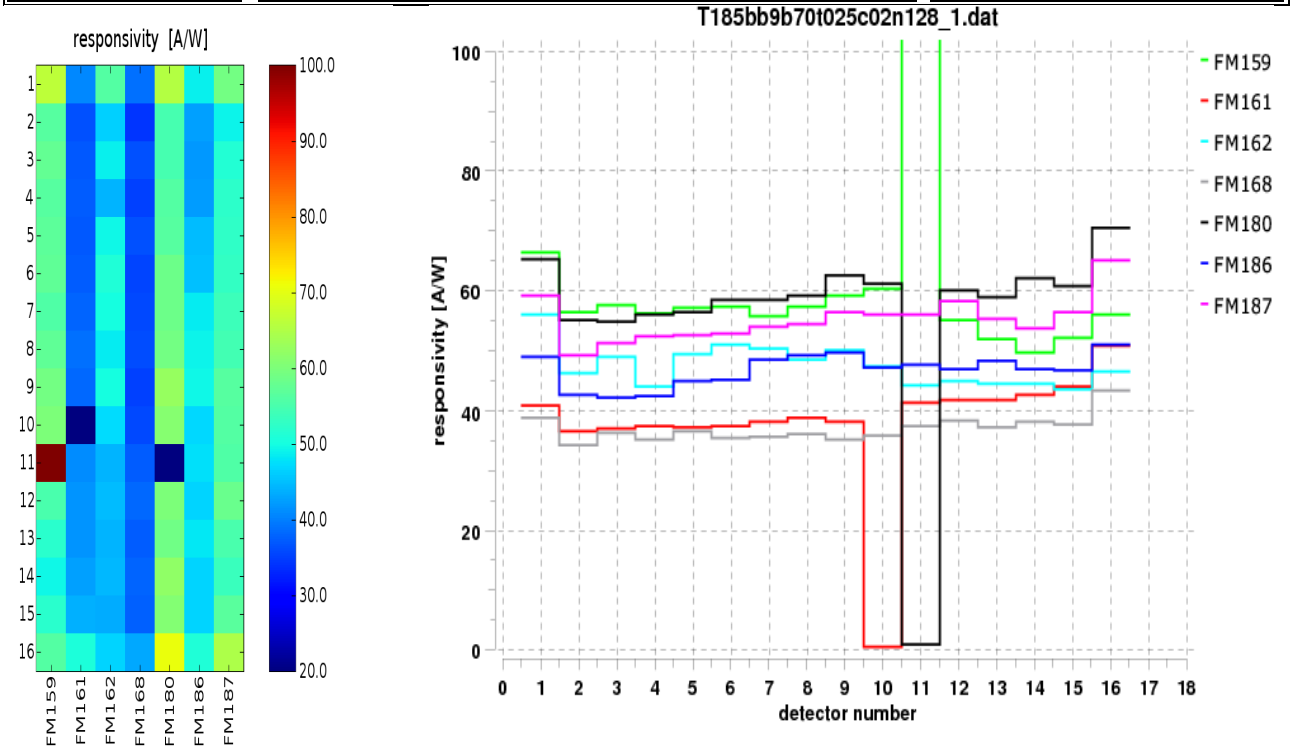

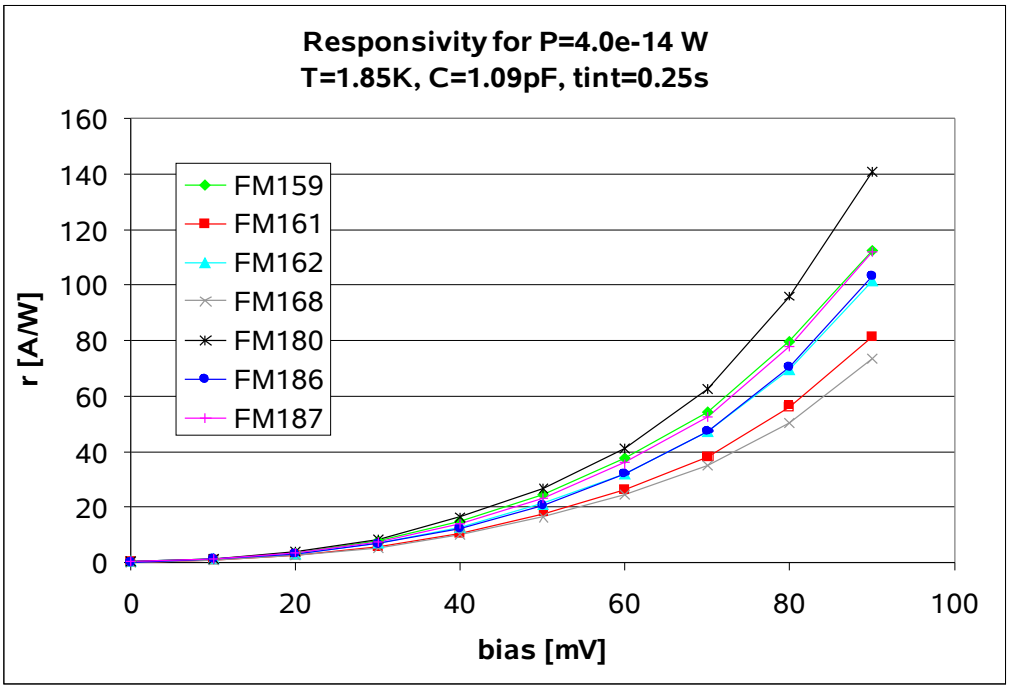

Fig. 22: *FM HS Sevenpack 5*: Open pixel in FM161 (pix 10) and FM180 (pix 11). Pixel 11 of module FM159 breakthrough at bias > 60mV.

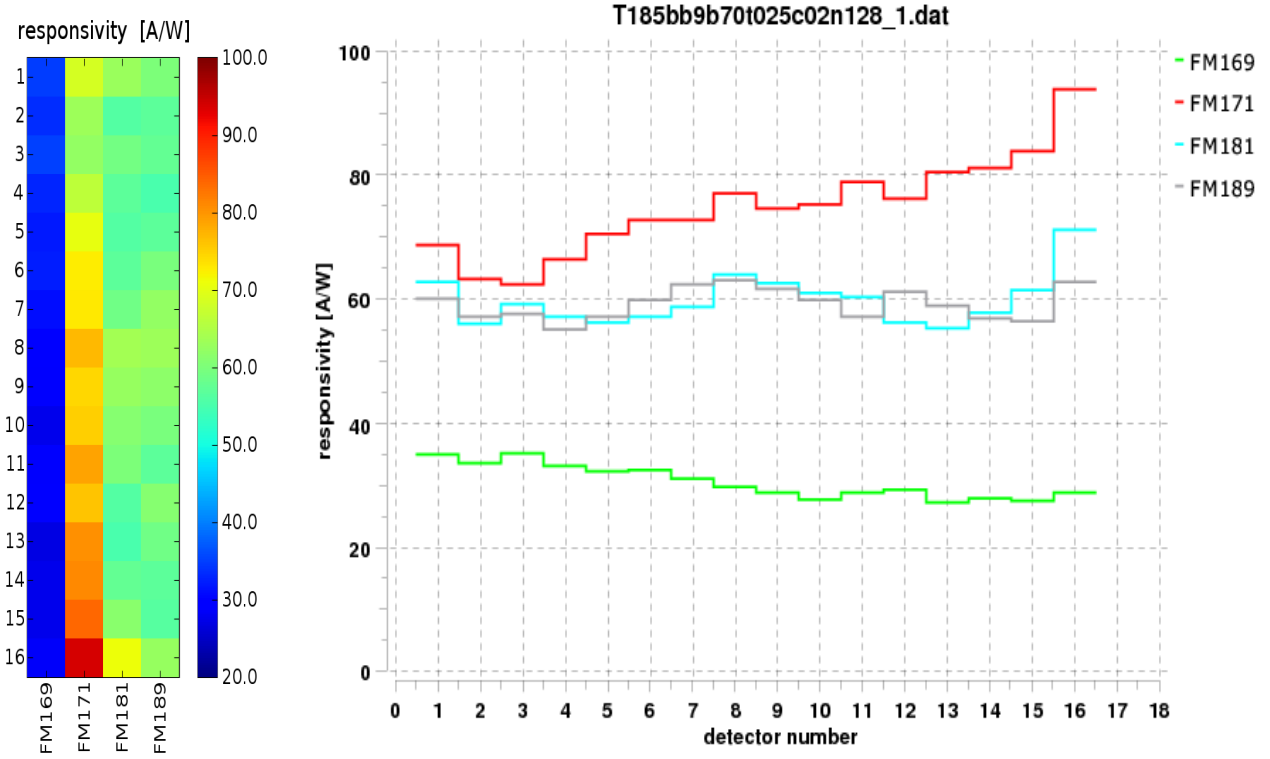

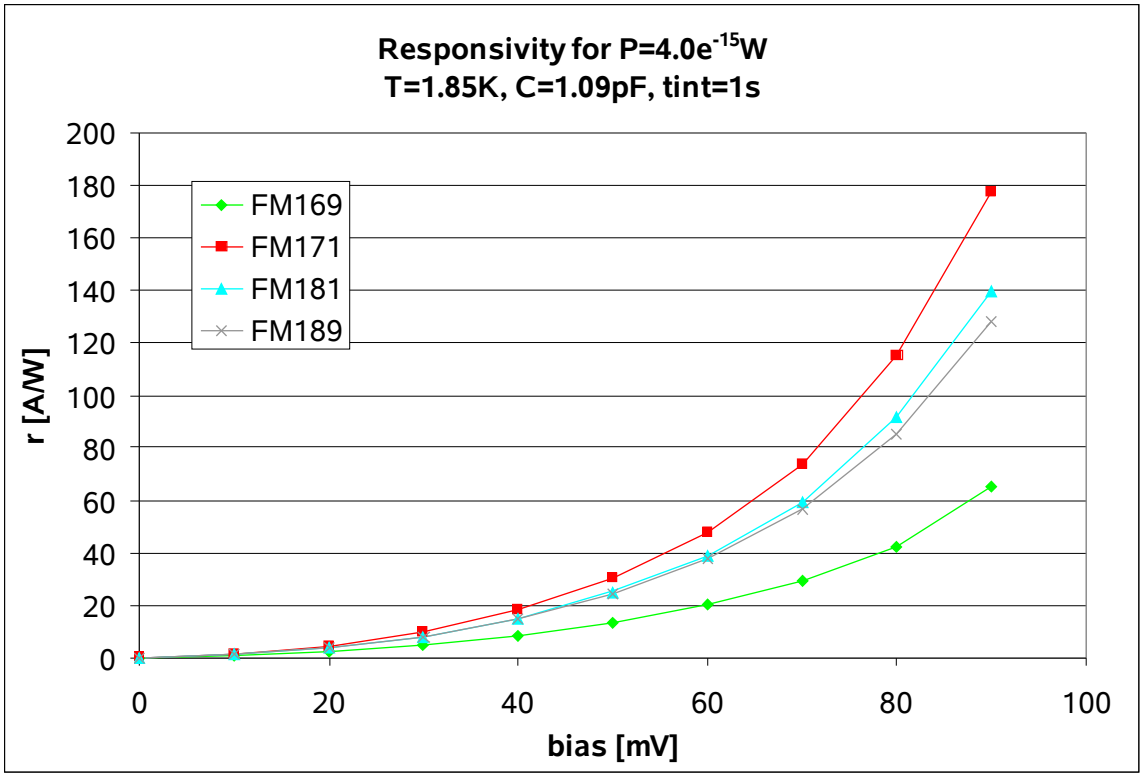

Fig. 23: *FM HS Sevenpack 6:*

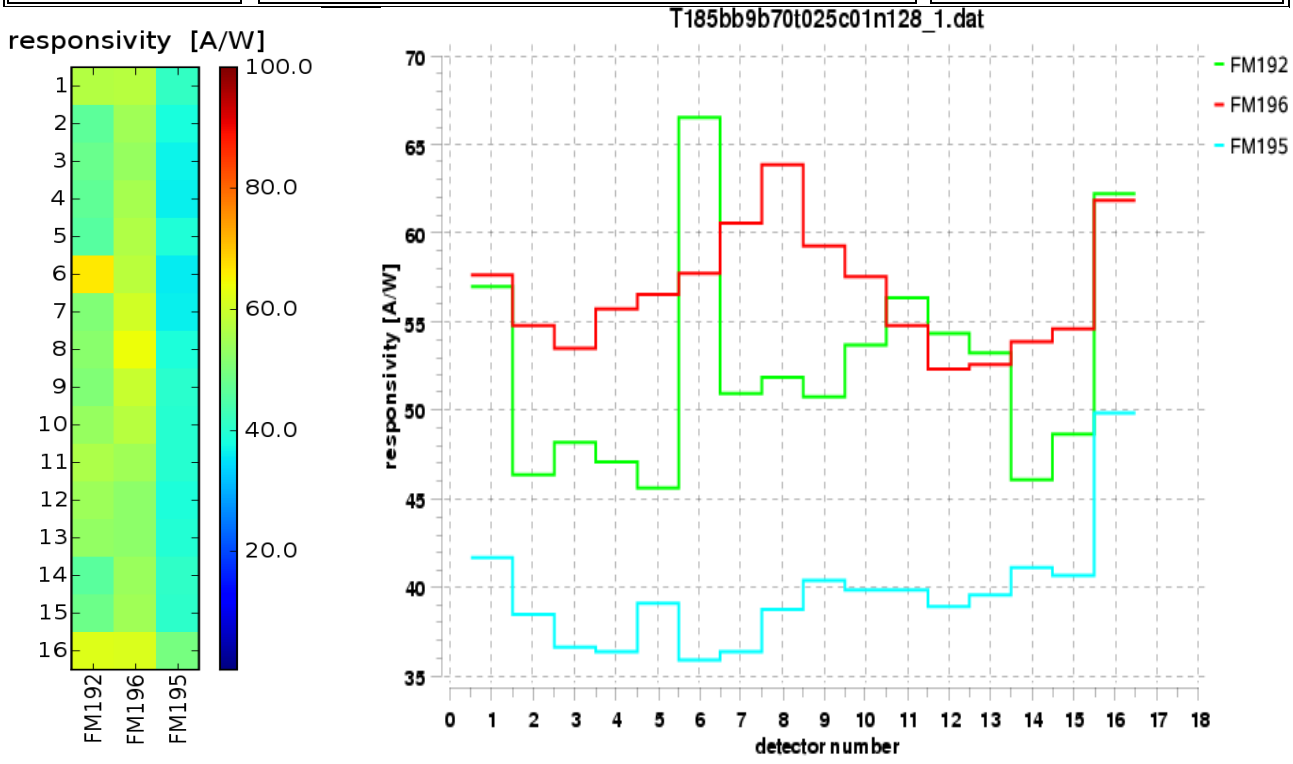

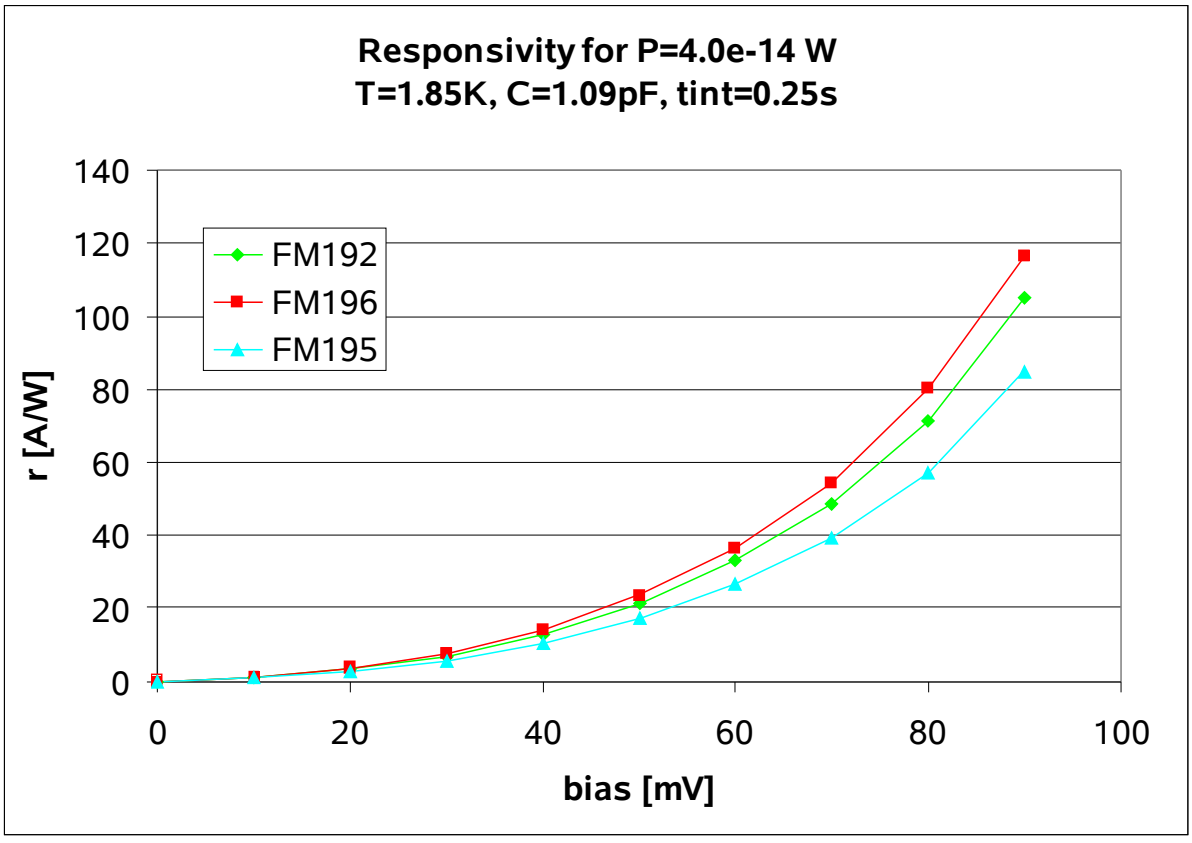

Fig. 24: *FM HS Sevenpack 10 (FM192 and FM196) and 11 (FM195)*

5.3.3 Homogeneity

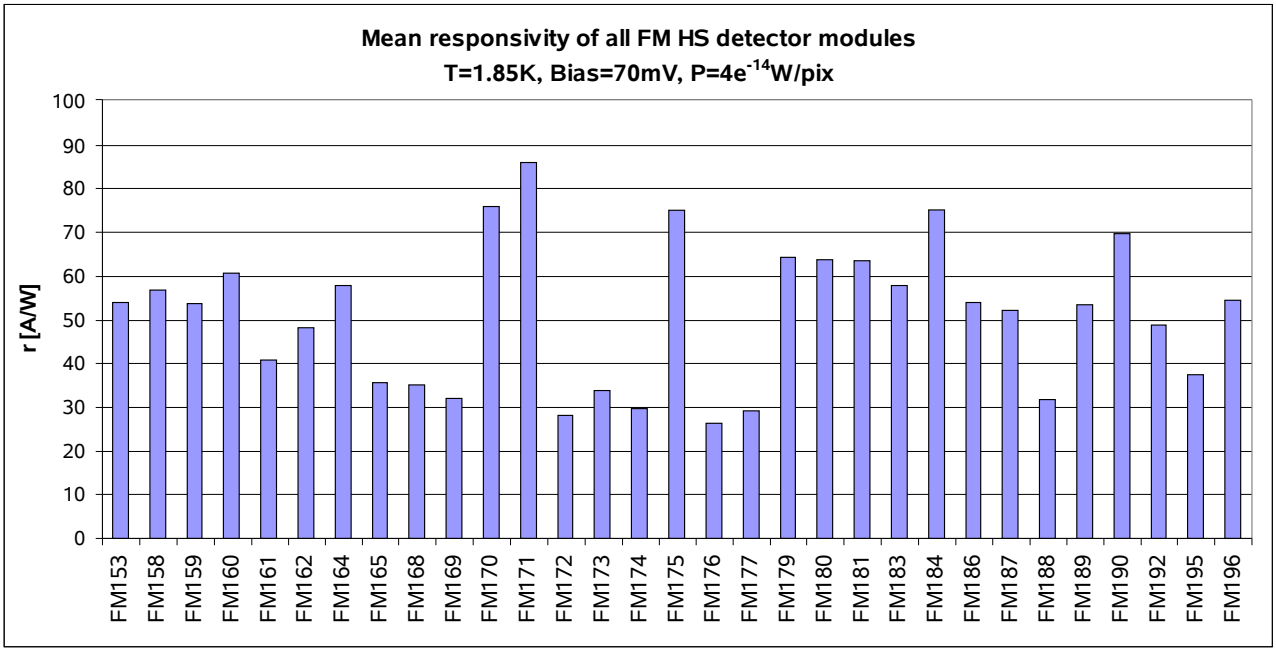

Fig. 25: mean responsivity of all FM HS modules

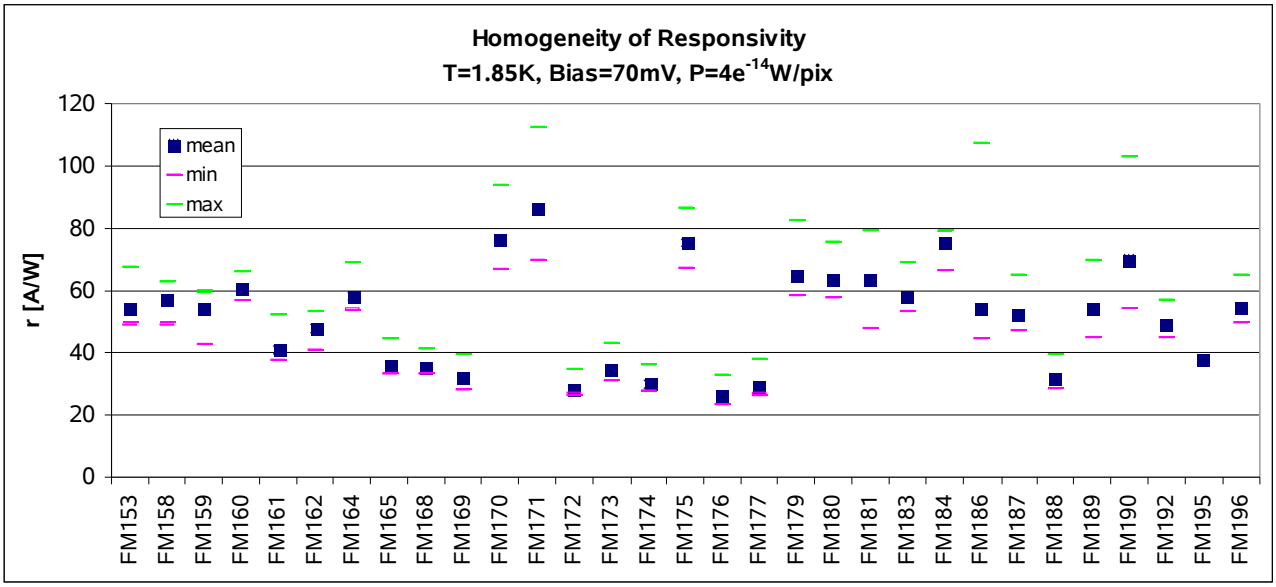

Fig. 26: mean responsivity and corresponding minimal and maximal values

We have to distinguish the homogeneity between all modules and within each module. The results of the modules with lowest and highest mean responsivity differ more than a factor of 3 (Fig. 25). In Fig. 26 the calculated mean responsivity and the corresponding maximum and minimum values are plotted. The most homogeneous module is FM160 with a calculated responsivity of 60A/W +8.6% / -6.7%, and the most inhomogeneous module is FM190 with 69A/W +47% / -22.6%. In general pixel 1 and 16 have a ~10% higher responsivity, because of the bigger collecting area of the light cones of the end pixels.

All types of "homogeneity" can be observed when comparing the responsivity distribution of the modules. Fig. 27 shows some examples, good homogeneity of FM174, slightly increasing and decreasing responsivity along the module in FM176 and FM169, "sine wave" like distribution in FM175 and a strong gradient in FM190. The strong increase along the detector stack in FM171 (and FM190), which is not caused by an inhomogeneous flux, cannot be explained.

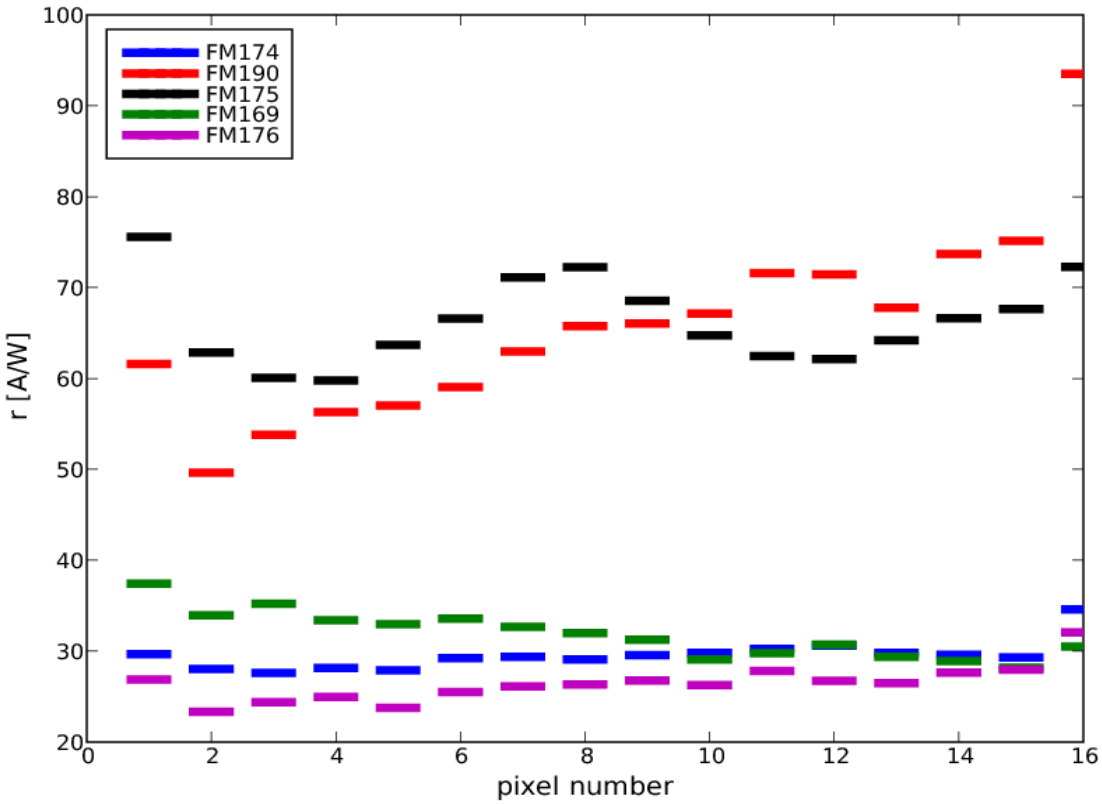

Fig. 27: Examples of "homogeneity"

The location of the pixels on the Ge:Ga waver has a weak correlation with the measured responsivity. The initial idea of the detector selection before the module assembly was to collect pixels with similar warm resistance for each module. In principle the higher the resistance of the detector pixel at room temperature, the higher the responsivity should be. From Fig. 28 one can derive, that beyond the warm resistance of the detector, at least the location of the pixel on the waver also has an influence on the responsivity. Detectors with a comparable resistance, but from a different location on the waver, show a wide range of responsivity.

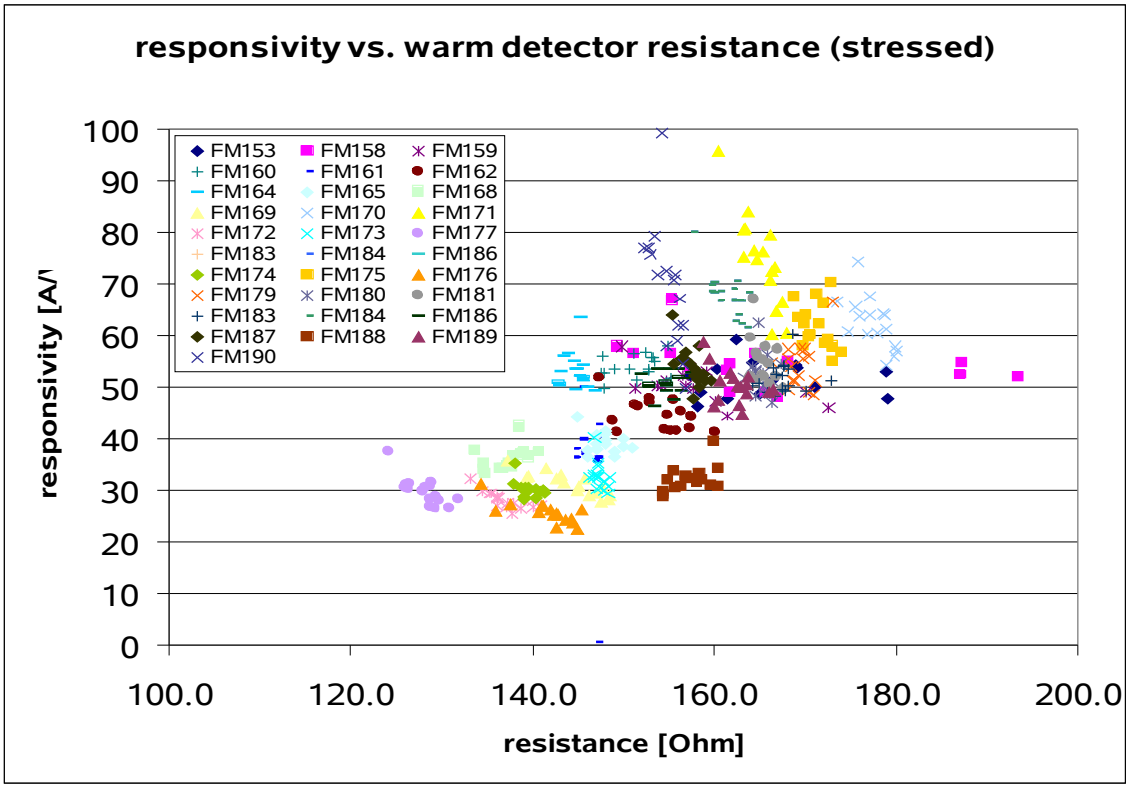

Fig. 28: measured responsivity vs. resistance of the high stress detectors at room temp.

5.3.4 Reproducibility

The reproducibility of the set-up was investigated by comparison of the signals of several modules measured during 10 test runs. Some modules were tested twice, FM153 three times. These modules were mounted at different positions within a Sevenpack each time. Fig. 29a to k shows the results of this comparison, the legend of each plot gives the number of the Sevenpack and the position within the test housing. In most cases the data fit very good together, which means that the reproducibility is within 10% or better. With the exception of FM168 and FM189 the curve progression of the signal along the module is equal. In FM168 and FM189 there are some deviations, maybe caused by work on both devices (FM168: re-gluing of wires on FEE, FM189: exchange of FEE) between the tests.

These results indicate that the test optics delivers a nearly homogeneous flux distribution at the entrance of the light cones of the tested modules.

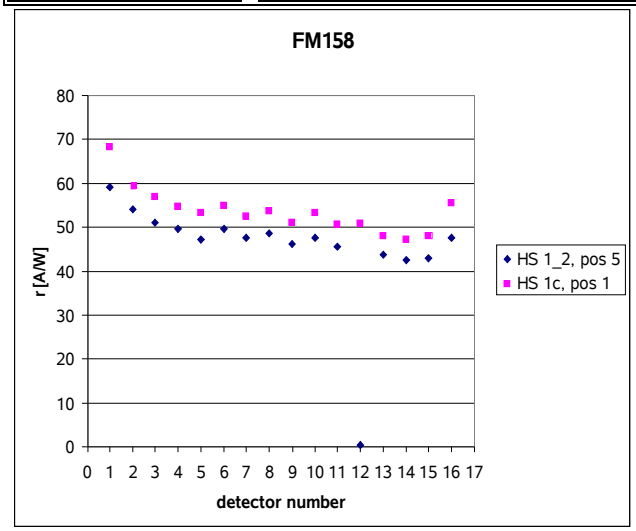

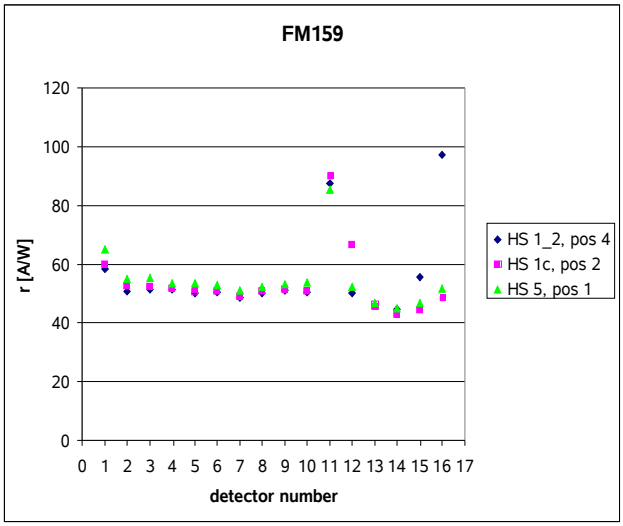

Fig. 29a,b

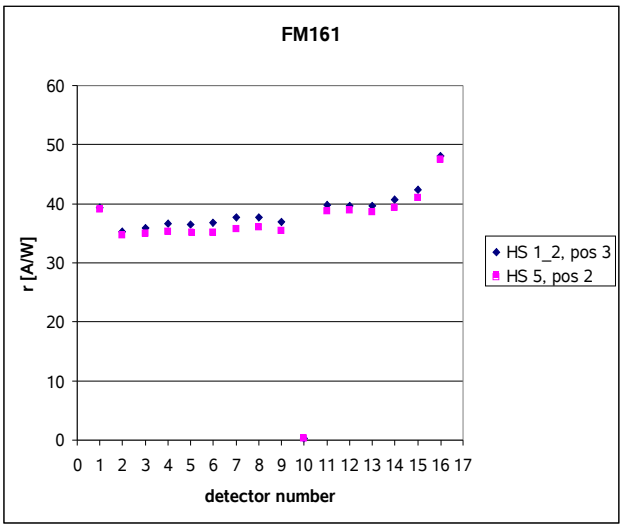

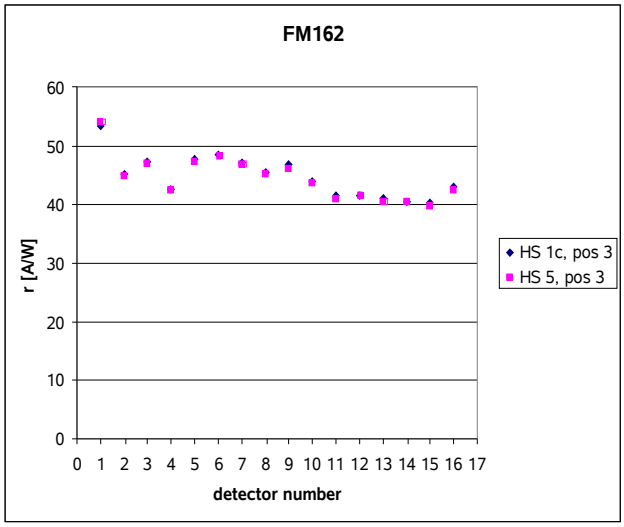

Fig. 29c,d

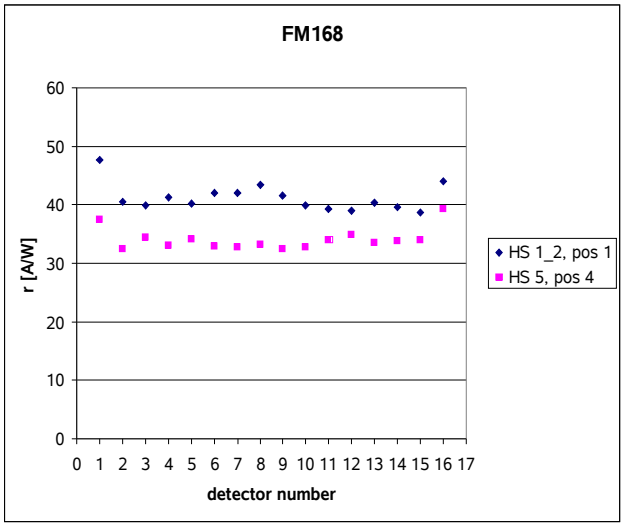

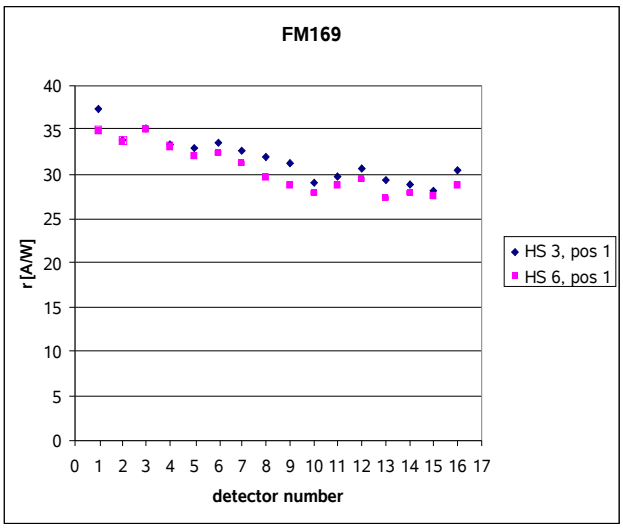

Fig. 29e,f

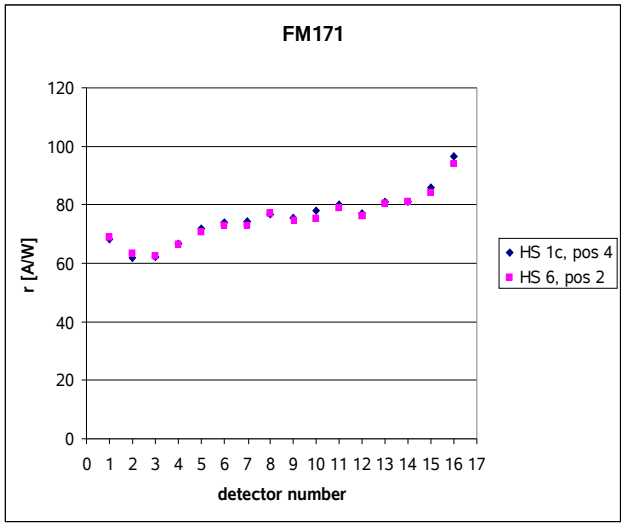

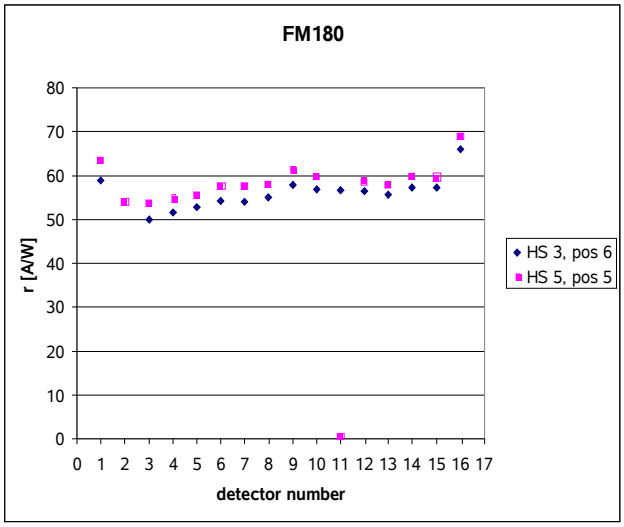

Fig. 29g,h

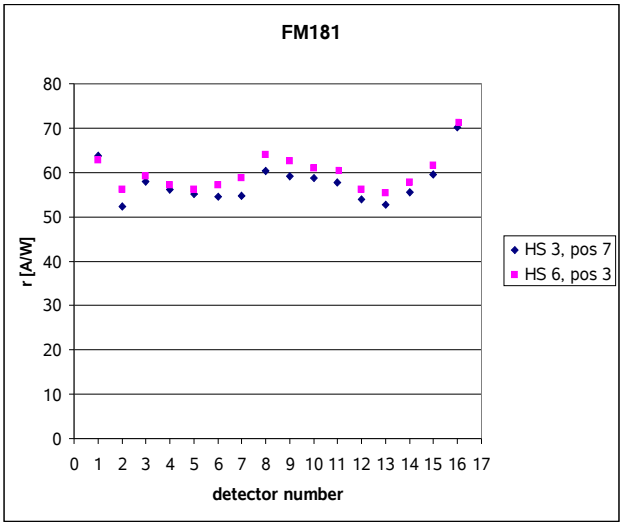

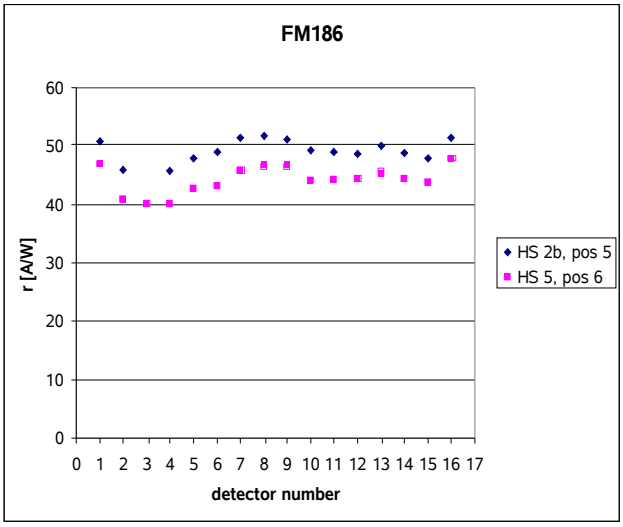

Fig. 29i,j

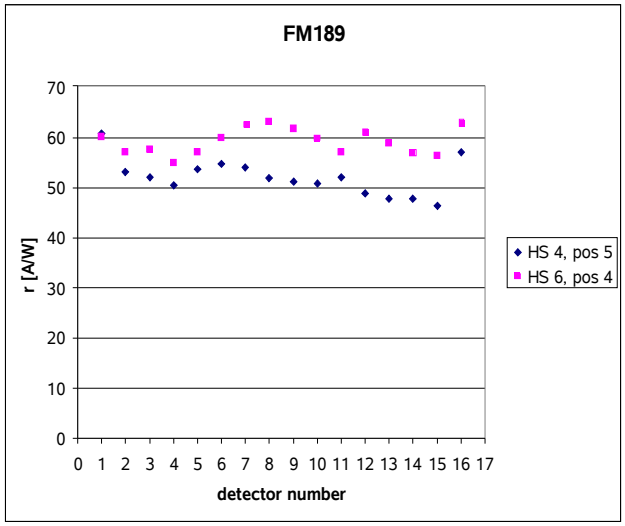

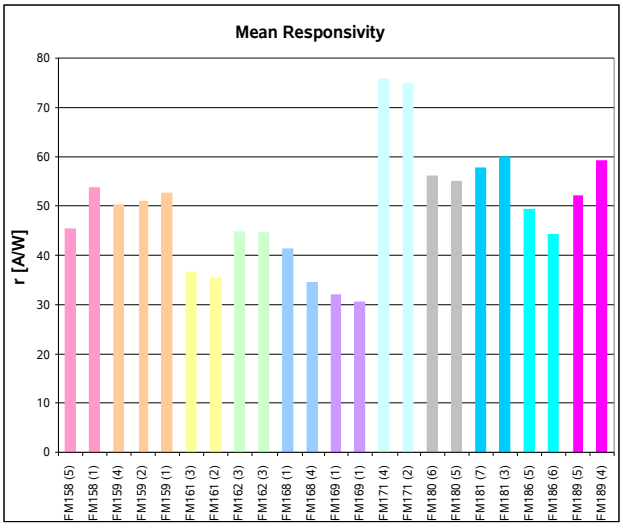

Fig. 29k,l

5.4 NEP

In this chapter the NEP of all modules in dependence of bias, integration capacity and flux level is shown.

The measured (total) NEP is defined as:

$$NEP_{tot} = \frac{\sqrt{2 \cdot tint} \cdot flux}{(\frac{signal}{noise})}$$

In general the measured NEP_{tot} of the modules includes the NEP_{RO} (determined by the CRE readout noise) and NEP_{BLIP} (photon noise limited) :

$$NEP_{tot} = \sqrt{NEP_{RO}^2 + NEP_{BLIP}^2}$$

At the flux levels used for presented data the $NEP_{tot} \approx NEP_{BLIP}$.

In Fig. 30 to 36 the calculated NEP of each Sevenpack at T=1.85K is plotted. Because of the presence of high noise caused by a ground loop during the test of Sevenpack HS3 no NEP data are available.

On each page the image of the NEP distribution and the corresponding line plot for a bias of 70mV and an integration time of 0.25s were shown. The adjusted photon flux was $4.2e^{-15}$ W per pixel. The smallest integration capacity was selected for all measurements. A fixed scaling was used in all plots for easy comparison of all modules. The lower plot on each page indicates the bias dependence of the mean value of all pixels (without open and strong pixels) for each module. During the test of Sevenpack HS6, a higher noise was present in the test set-up for unknown reason, which led to a higher calculated NEP for included modules (Fig. 35)

While the lowest NEP measured at this flux level was about $1e^{-17}$ W/√Hz, the minimum NEP of $0.8e^{-17}$ W/√Hz were reached at a flux level of $2.4e^{-15}$ W per pixel, which is expected to be near the NEP_{RO}.

The dependence of the NEP on the selected integration capacity is show in Fig. 37 and 38. Compared with the QM modules, where the lowest NEP was measured with the second smallest integration capacity, the FM modules show the lowest NEP with the smallest integration capacity. The minimum NEP was reached at different bias voltages (around 70mV for FM171 and 80mV for FM174), depending on the responsivity of the modules (FM171 has a 2.5 times higher responsivity than FM174).

In Fig. 39 and 40 the NEP of FM177 and FM184 at various flux levels is plotted. The integration time was 0.25s and the integration capacity 0.14pF. The flux was changed by a factor of 17 from $2.4e^{-15}$W to $4.0e^{-14}$W. For both modules, the minimum NEP for the lowest flux is $8e^{-18}$W/√Hz. It was reached at different bias voltages, at 70mV for FM184 and 90mV for FM177, depending on the responsivity.

5.4.1 Dependence on Bias

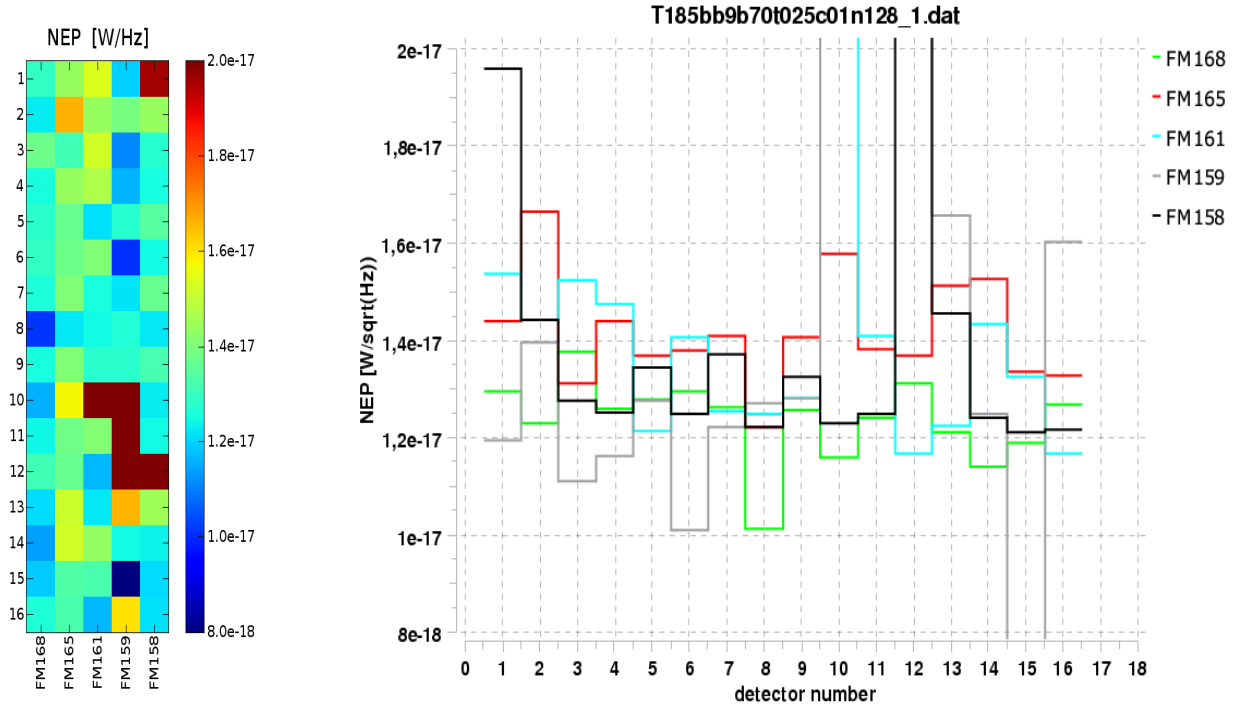

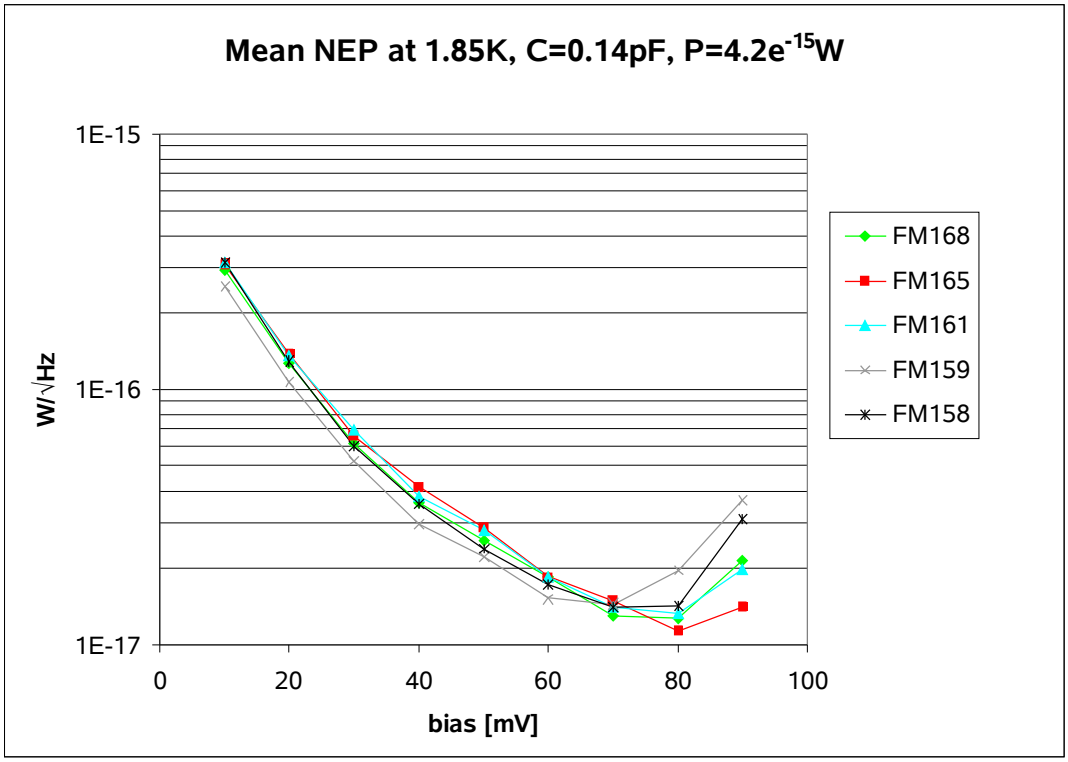

Fig. 30: *FM HS Sevenpack 1(2)*: Open pixel in module FM158 (pix 12) and FM161 (pix 10). In module FM159 pixel 11 break through at bias > 60mV and pixel 16 has a high signal without break trough up to 90 mV.

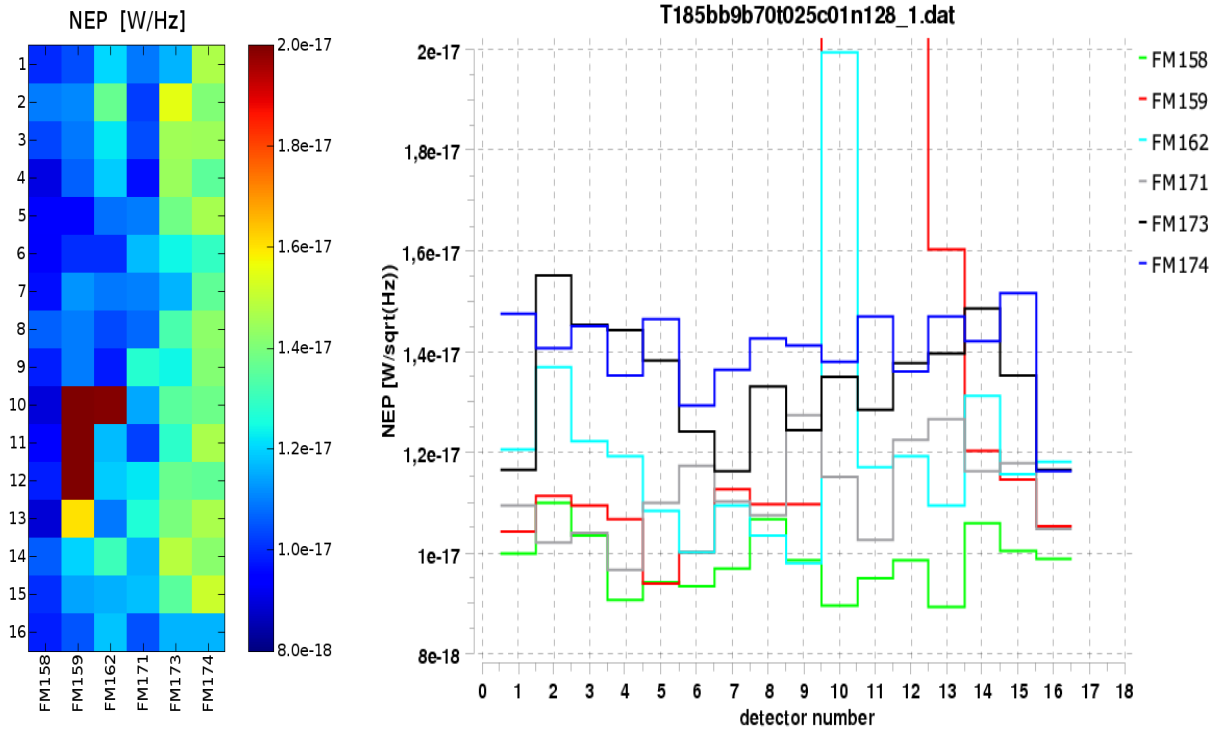

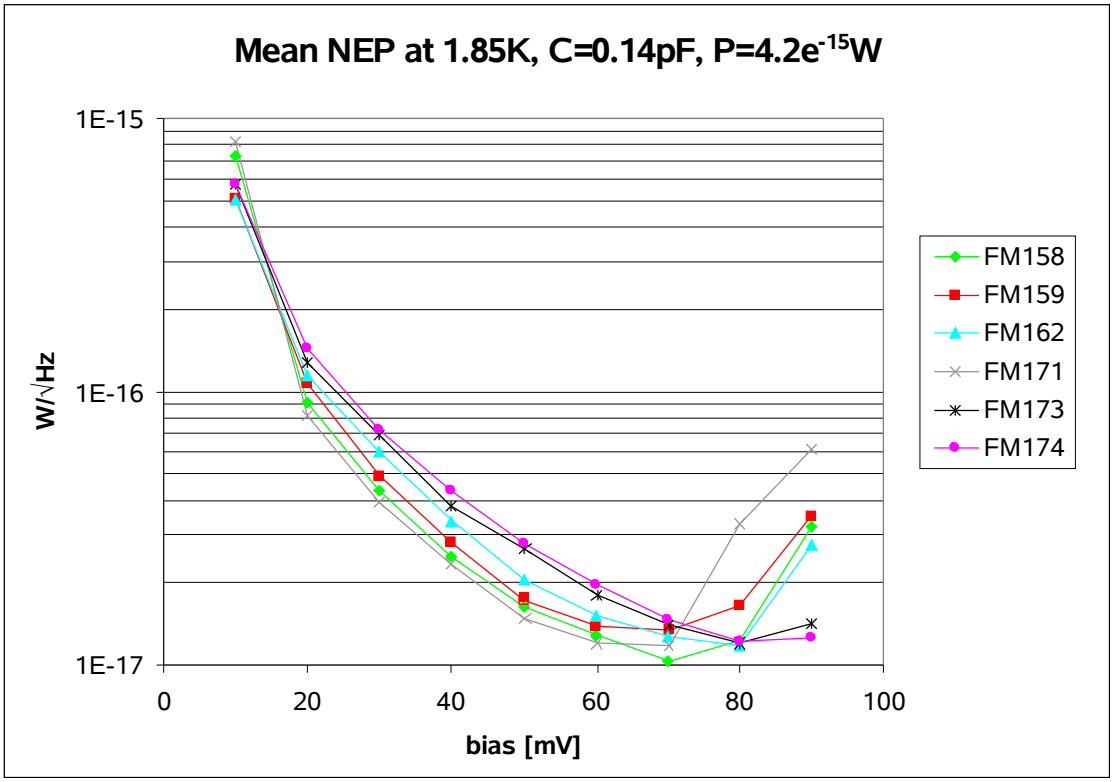

Fig. 31: *FM HS Sevenpack 1c*: Pixel 11 and 12 of FM159 break through for bias > 60mV. Different behavior of pixel 12 and 16 in comparison with FM Sevenpack HS1(2). Higher noise and NEP in pixel 10 of FM162

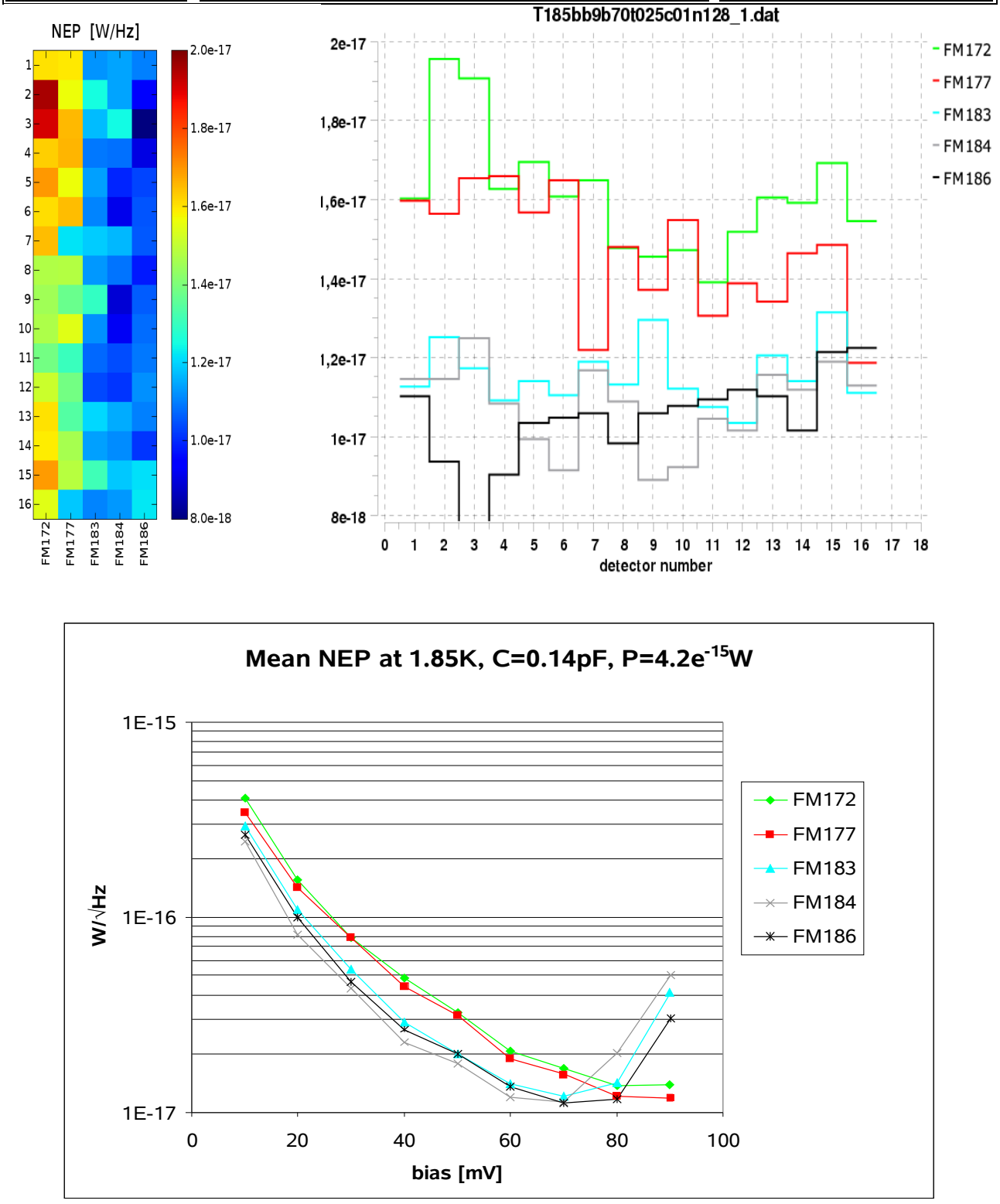

Fig. 32: *FM HS Sevenpack 2b*: Pixel 3 of FM186 has a very low NEP, because of a extreme high signal current, which is not created by the detector, but most probably an effect of the CRE/FEE.

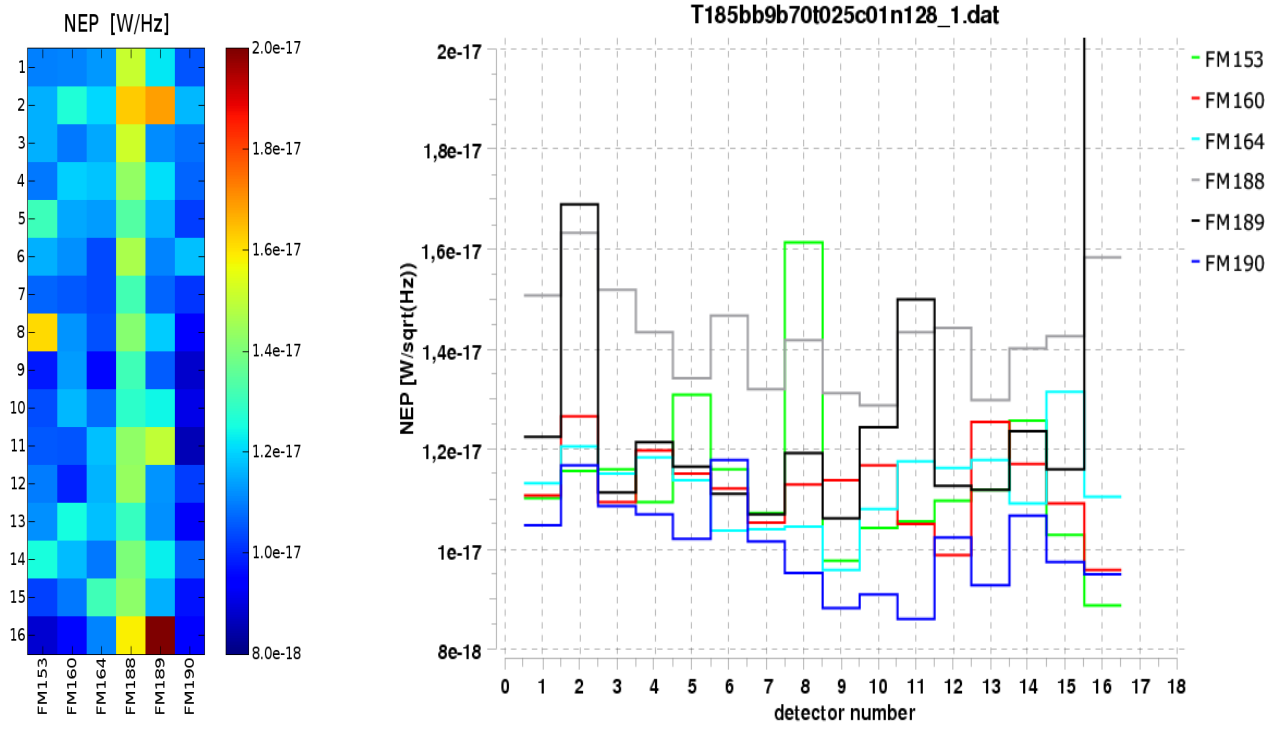

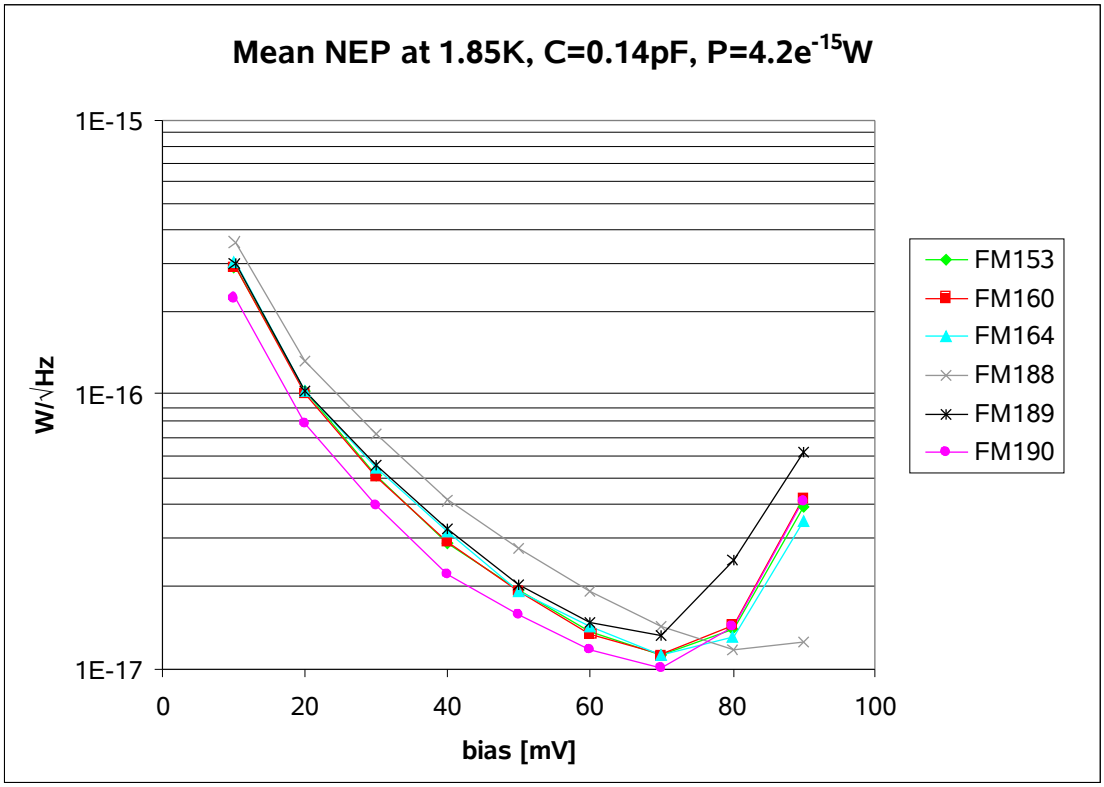

Fig. 33: *FM HS Sevenpack 4:* Pixel 16 of FM190 shows a high NEP

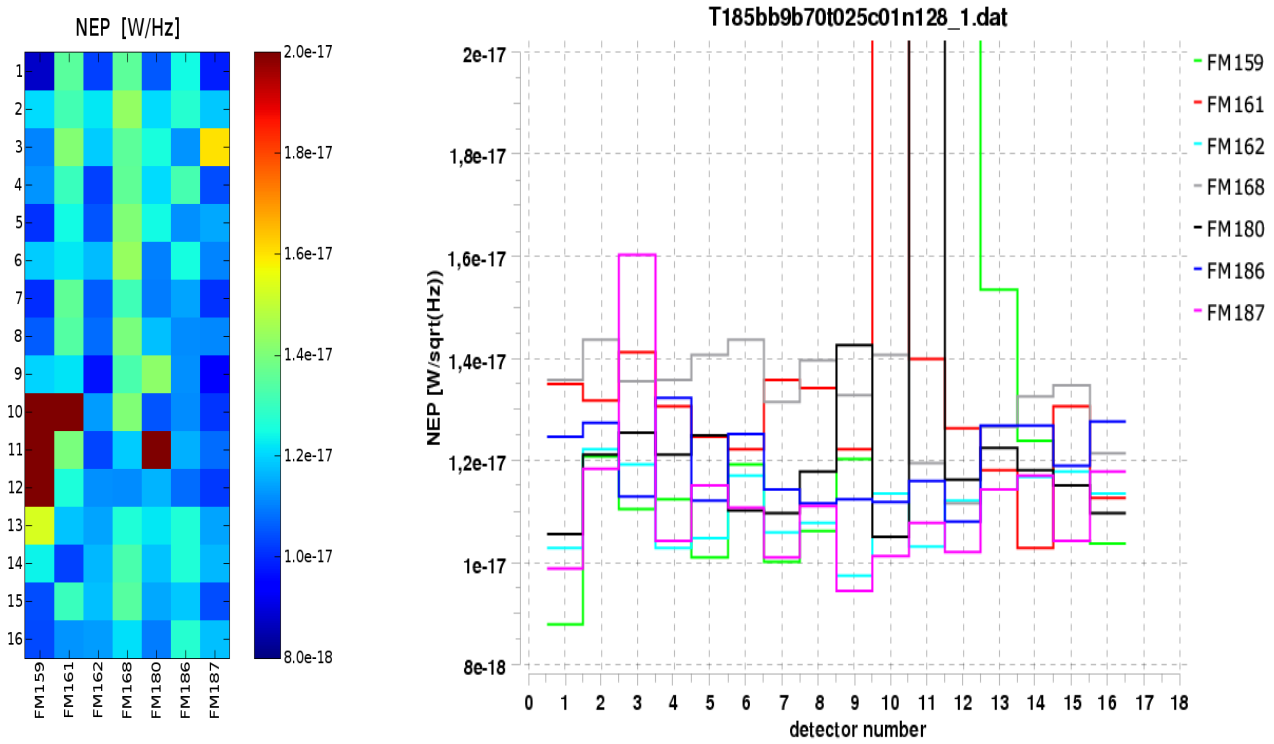

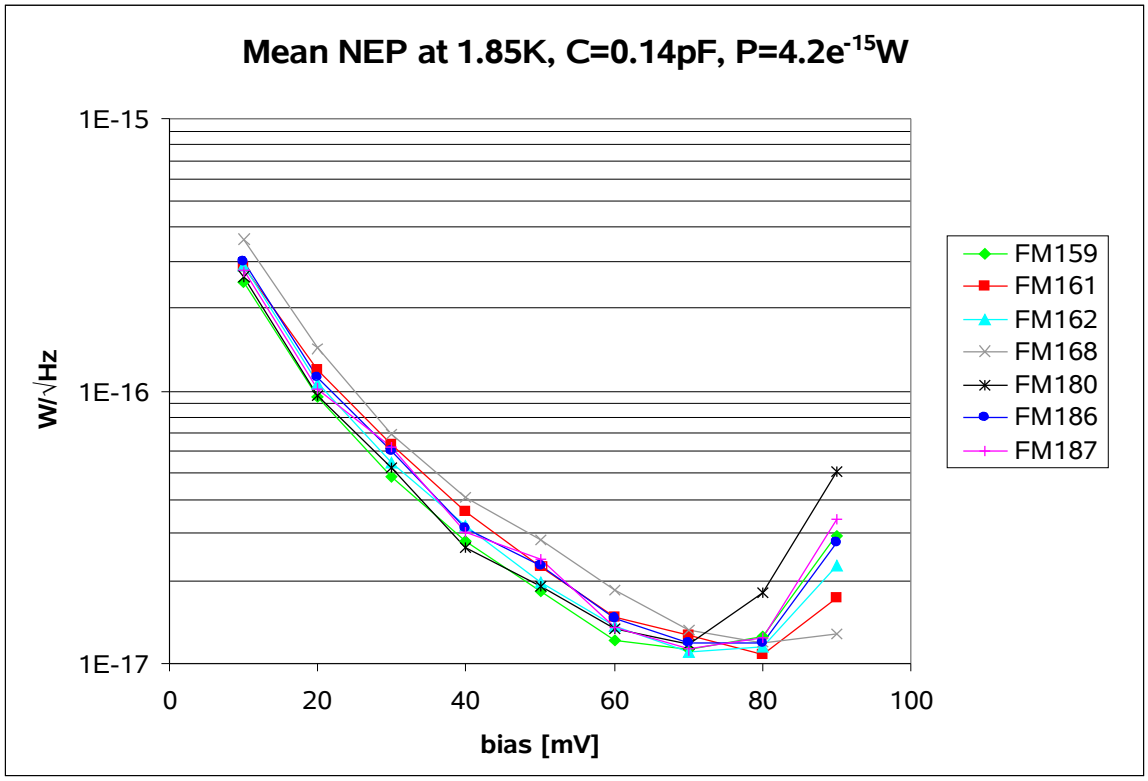

Fig. 34: *FM HS Sevenpack 5:* Open pixel in FM161 (pix 10) and FM180 (pix 11). Pixel 11 of module FM159 breakthrough at bias > 60mV.

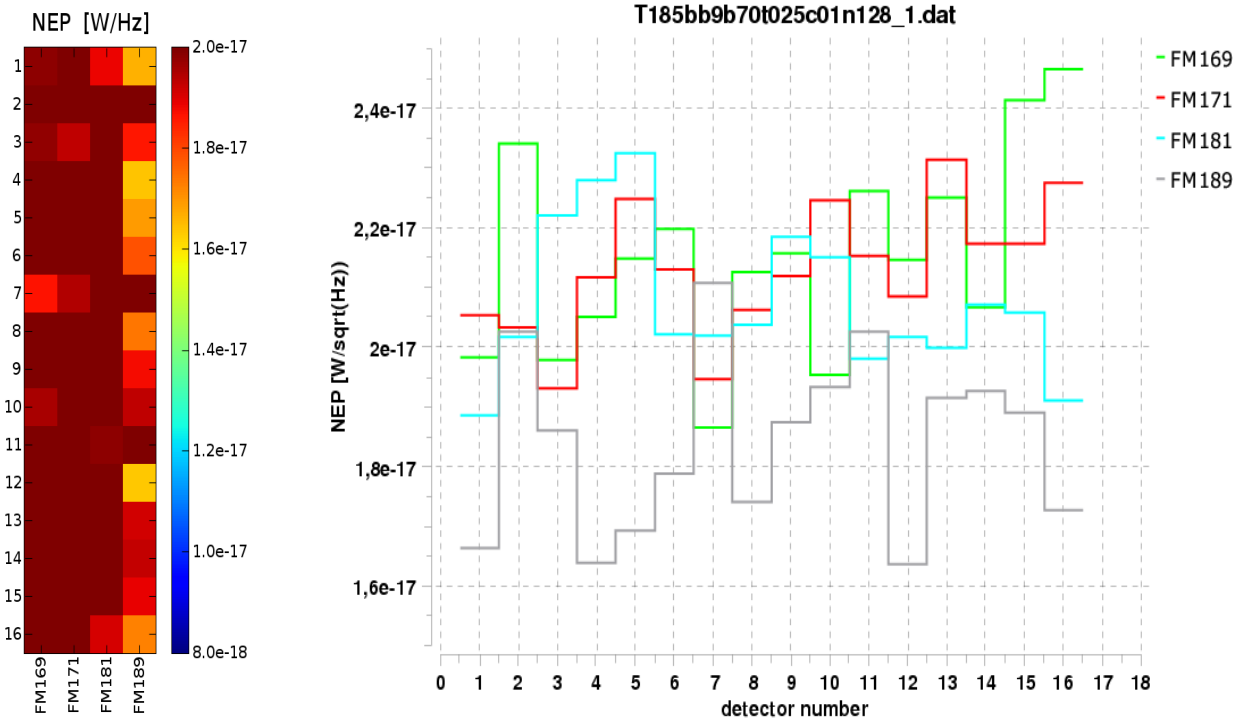

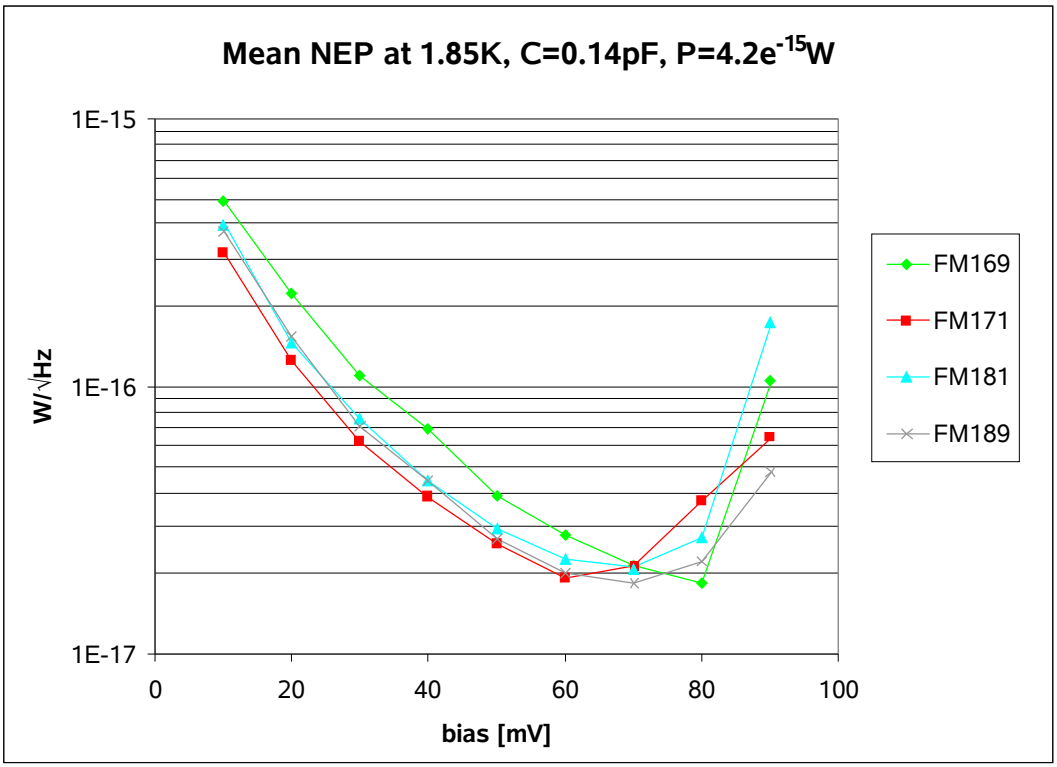

Fig. 35: *FM HS Sevenpack 6:* Up to a factor 2 higher noise than in the other Sevenpacks for unknown reasons, but not from the test set-up.

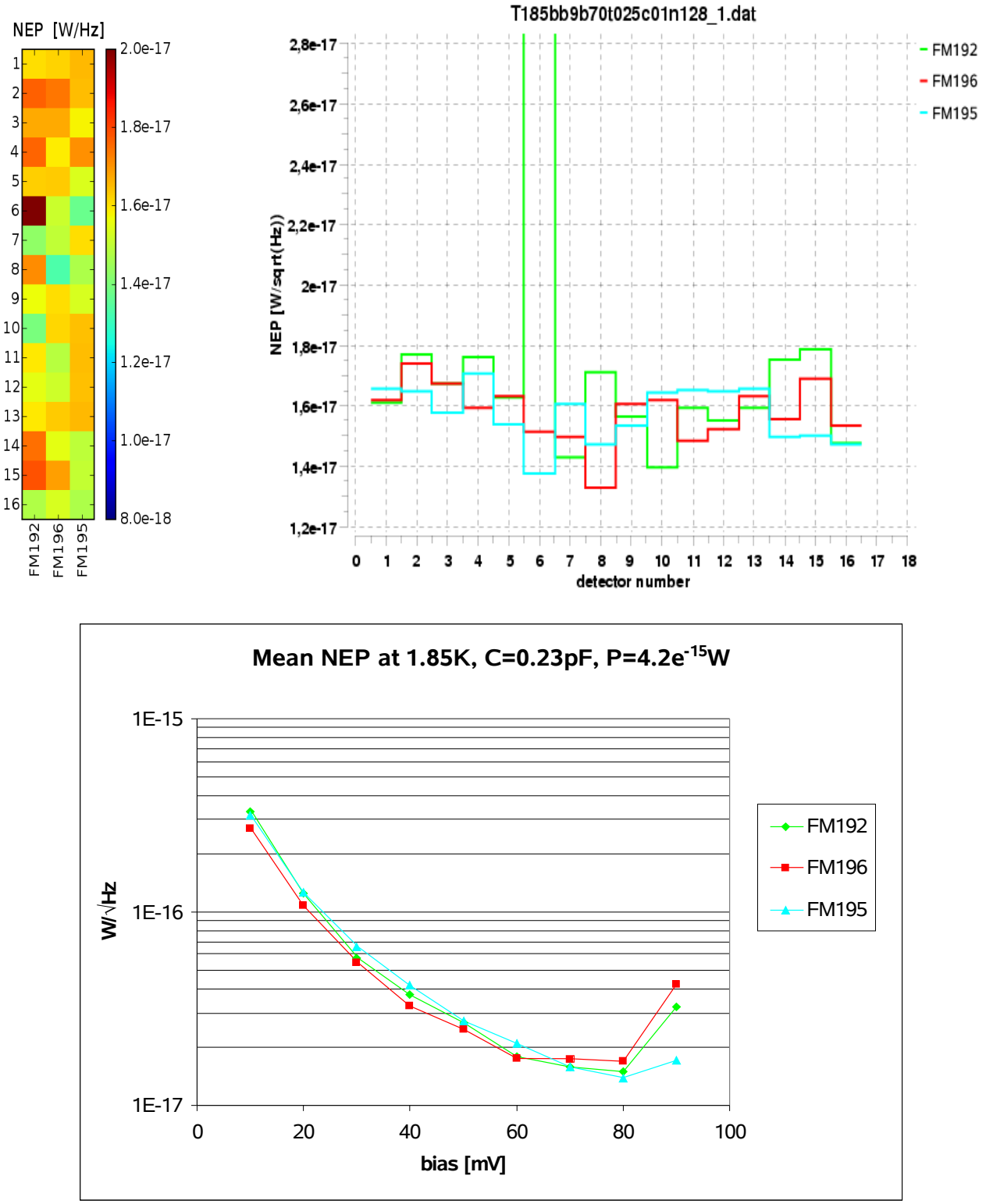

Fig. 36: *FM HS Sevenpack 10 (FM192 and FM196) and 11 (FM195):* high NEP in pixel 6 of FM192

5.4.2 Dependence on Integration Capacity

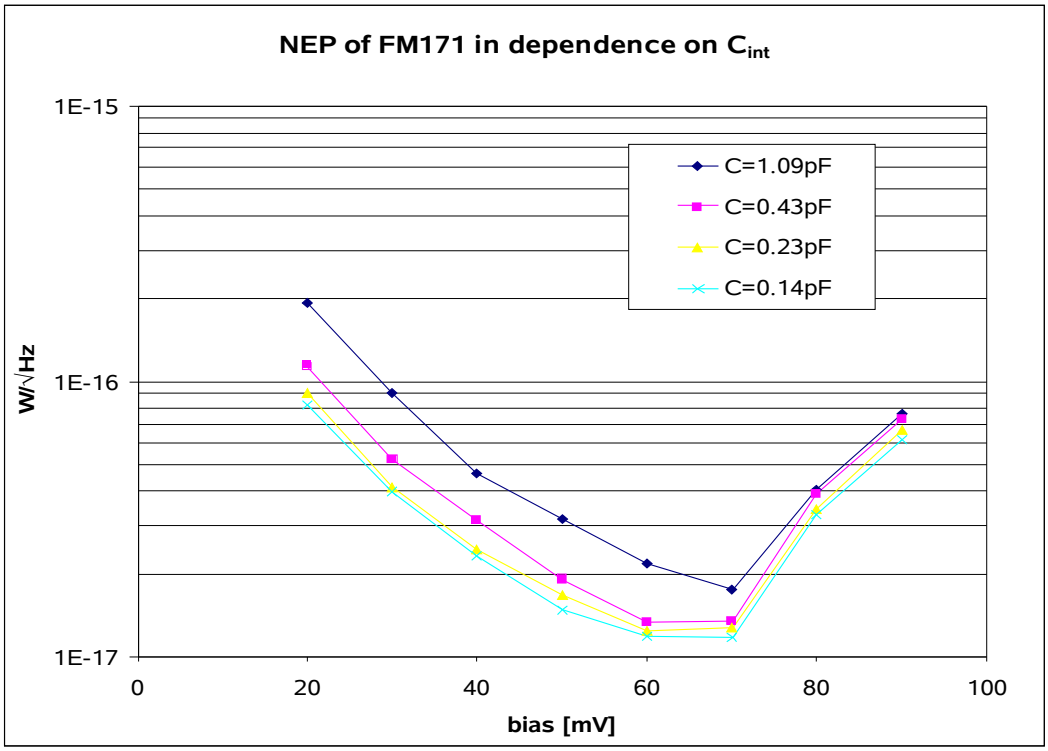

Fig. 37: NEP of FM171 for various integration capacities

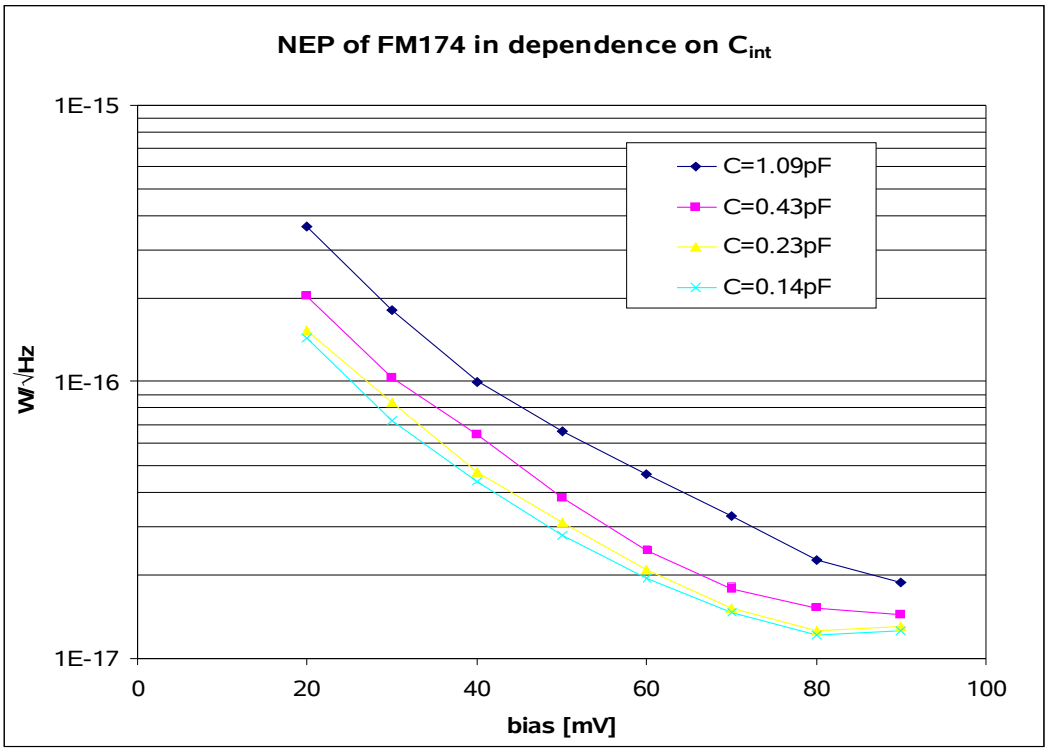

Fig. 38: NEP of FM174 for various integration capacities

5.4.3 Dependence on Flux

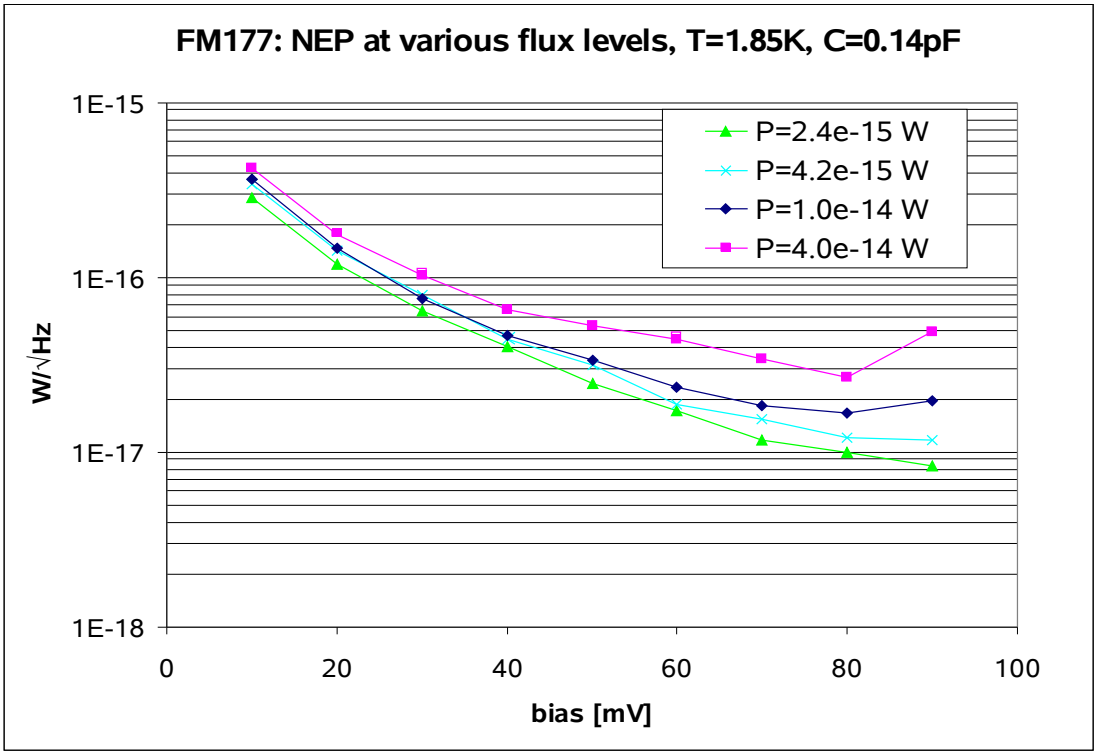

Fig. 39: NEP of FM177 for various flux levels

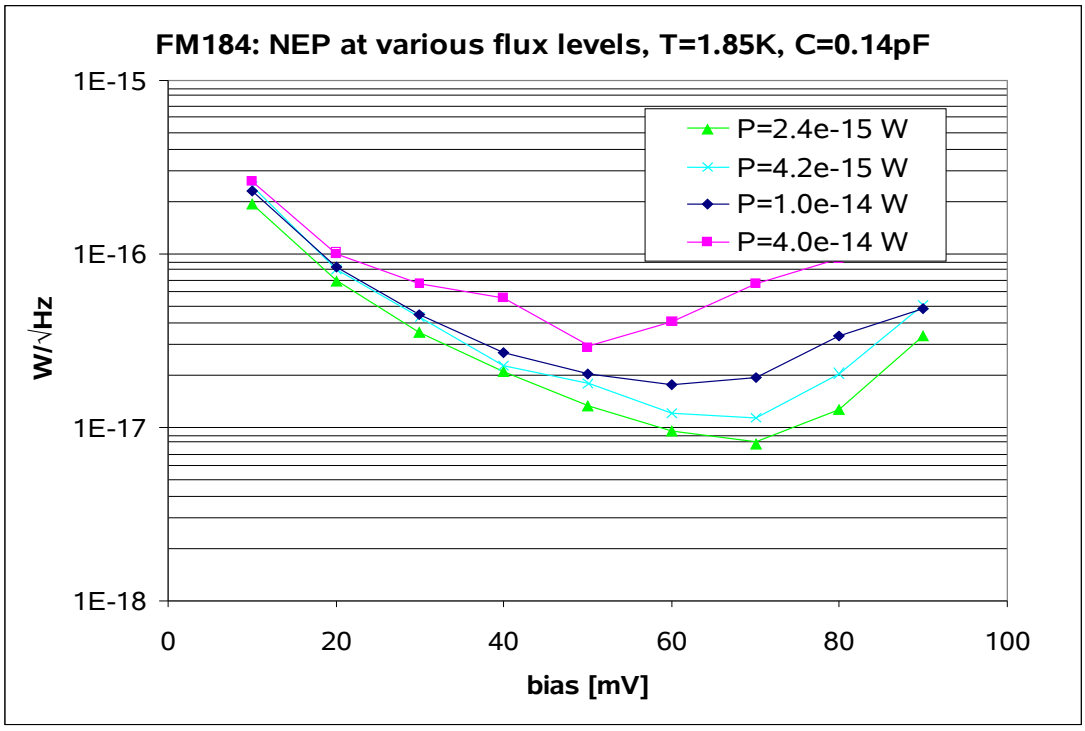

Fig. 40: NEP of FM184 for various flux levels

5.5 Signal Dependence on Integration Time

In Fig. 41 the calculated responsivity of pixel 2 from FM171 for a bias of 50mV is plotted versus the integration time. The plot shows a decrease of the responsivity from 26.3 A/W to 24.4/W between 1/16 s and 2 s integration time, which is a change of about 8%.

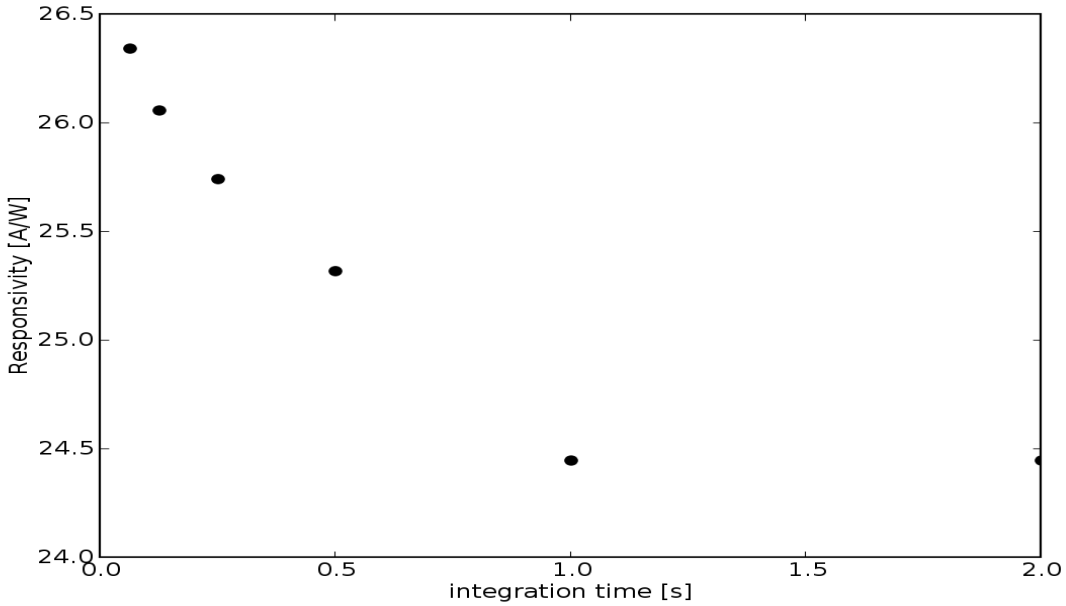

Fig. 41: Responsivity of pixel 2 from FM171 at bias=50mV versus integration time

The main reason for this responsivity change is the stronger de-biasing of the detectors with longer integration times. Another possible influence comes from a not 'perfect' reset. The reset level (voltage where the detectors start integration after a reset) also depends on the integration time. The shorter the integration time the higher the reset level and probably the effective bias voltage. This effect is demonstrated with the plots of Fig. 42.

The upper plot shows 6 ramps with integration times from 1/16s to 2s: the ramps have the same slope.

In the plot below the linear fit of each ramp is drawn. All fit curves were extrapolated to 2s for better comparison. One can clearly see that the slope depends on the integration time.

The 3rd and 4th plot show the raw data and the linear fit of the first 1/16s of each ramp. The change of the reset level is about 30mV between short and long integration time. A hook at the beginning of the ramp is present for the longer integration times. Again, one can see the different slope of the fits at the first 1/16s of the ramps, where the de-biasing has still no influence, and the hook is only partly responsible for the smaller slope of the ramps with longer integration time.

At the lowest figure the calculated slope of the complete integration ramps (red square) and the slope of the first 1/16s of each integration (blue circle) is plotted.

All investigated examples show this behavior.

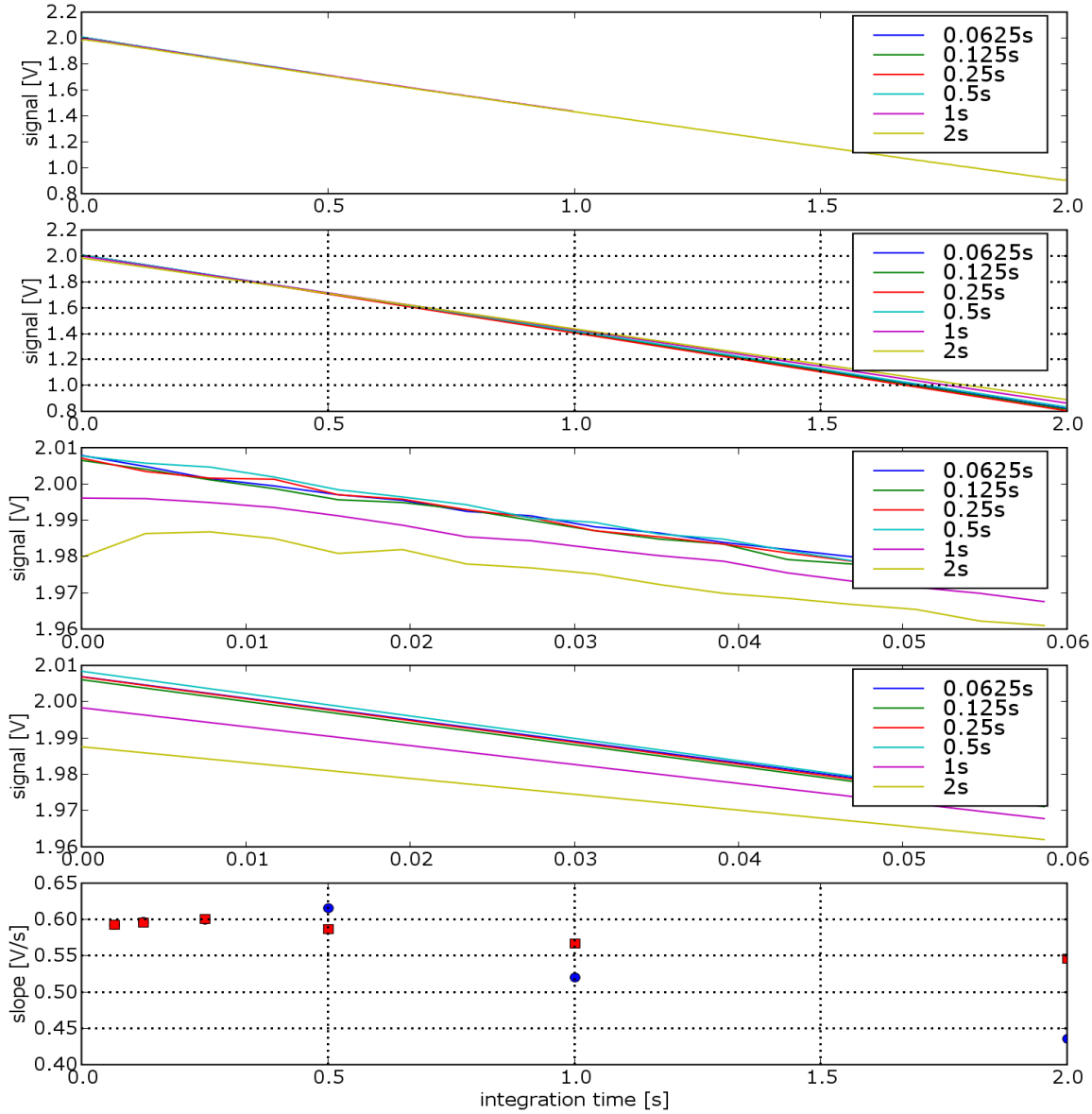

Fig. 42: Raw data of 6 integration ramps with t_{int}=0.0625s to 2s

linear fit of raw data (fit extrapolated to 2s)

first 1/16s of each raw data

linear fit of the first 1/16s of each raw data

calculated slope of the complete ramp (red square) and of the first 1/16s of each ramp (blue circle)

If the integration ramps (with different integration times) are divided in sub-ramps of length 1/16s, and the slope of each sub-ramps is calculated, one gets the result shown in Fig. 43, where the slope of the sub-ramps versus sub-ramp number is plotted. The big difference of the slope for the lower sub-ramp numbers is due to the hook at the beginning of the integration ramps with longer integration time. The decrease of the slope with higher sub-ramp number is caused by de-biasing.

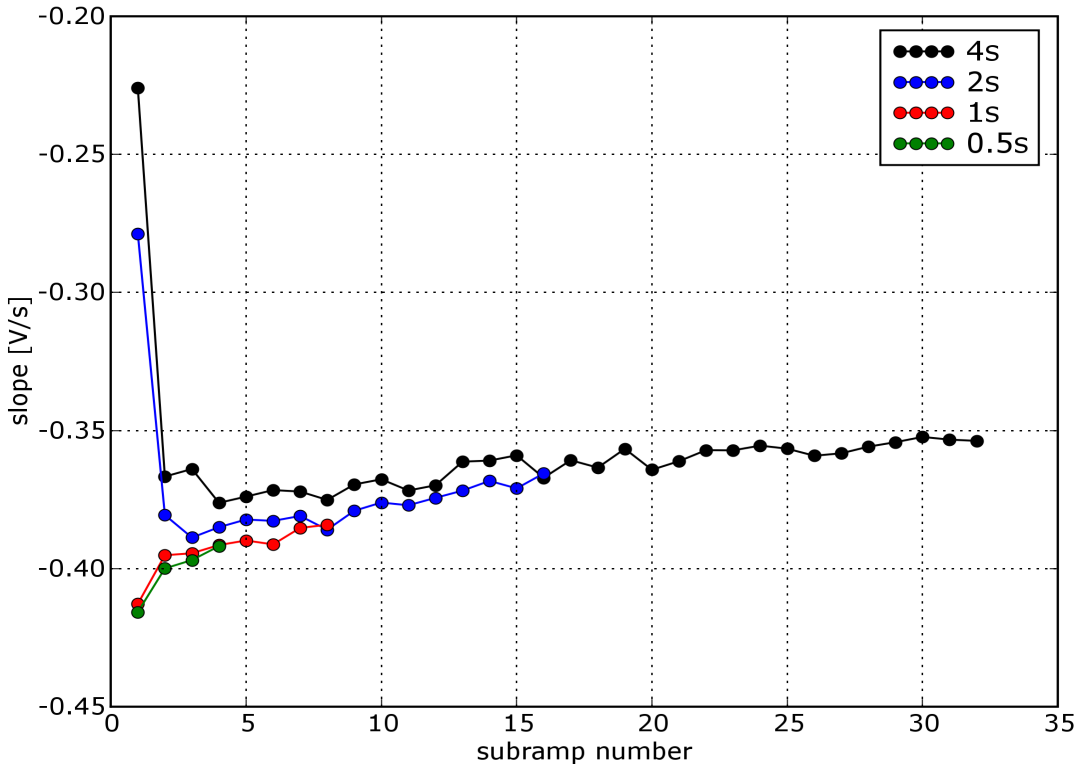

Fig. 43: slope of sub-ramps versus sub-ramp number for different integration times (pixel 10 of FM192)

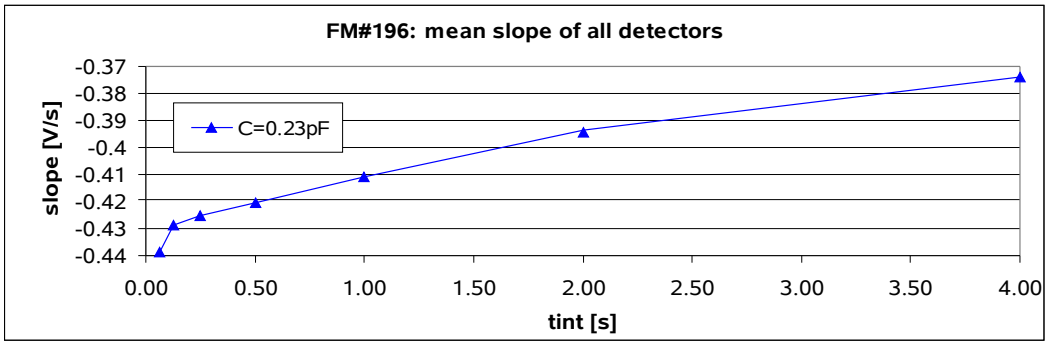

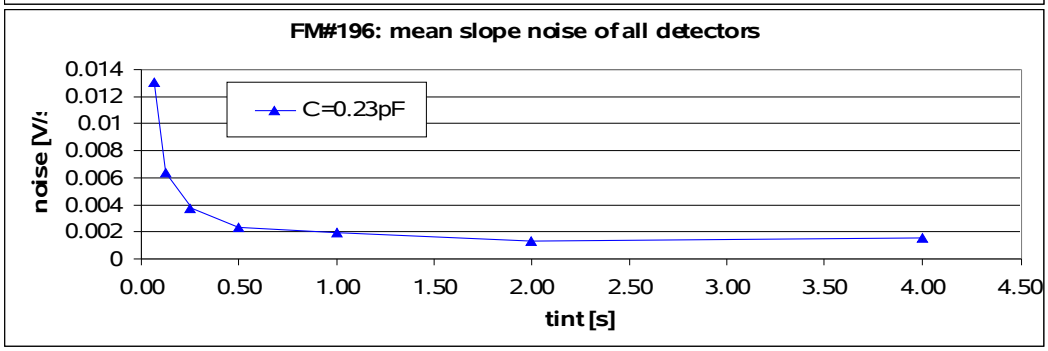

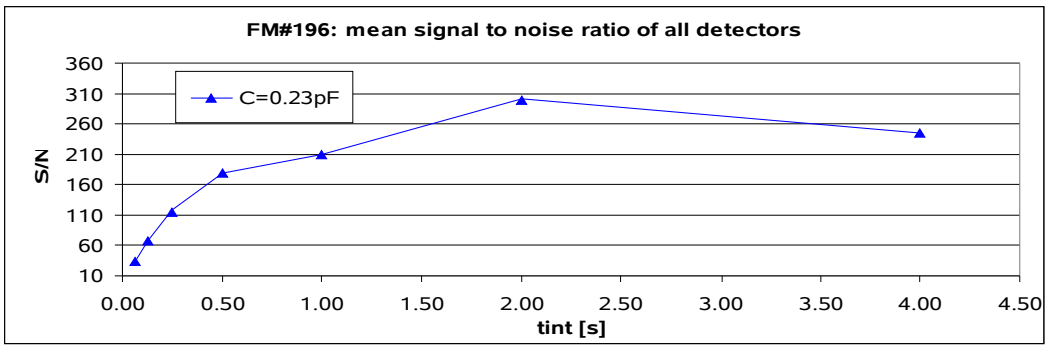

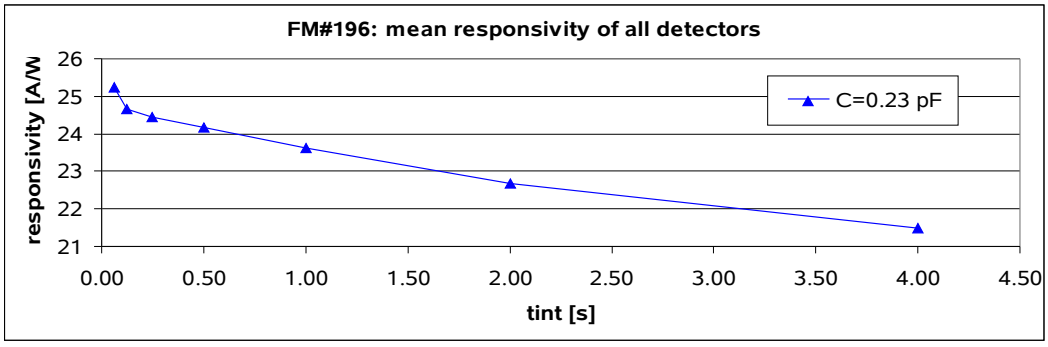

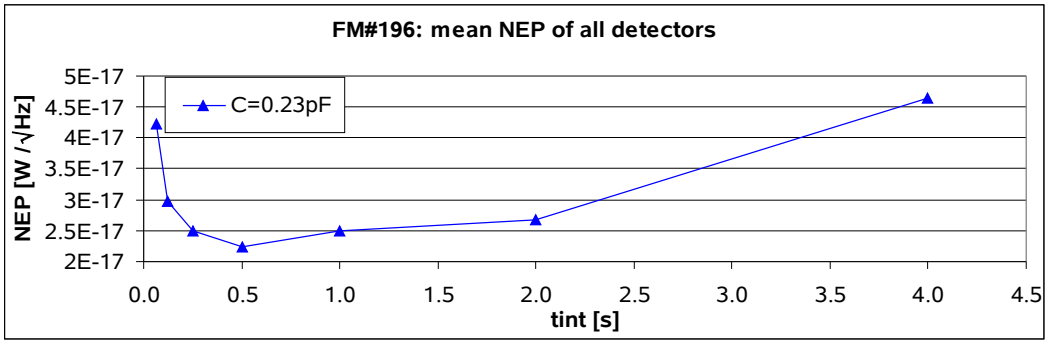

Fig. 44: slope, slope noise, S/N, responsivity and NEP of FM196 versus tint

Fig. 44 demonstrates the integration time dependence of the slope, slope noise, signal to noise ratio, responsivity and the NEP of FM196 for a bias of 50mV at T=1.85K. The complete measurement time at each integration time was 64s, the number of ramps between 0.0625s and 4s changed from 1024 to 16 respectively. While the maximum signal to noise ration is reached for tint=2s, a minimum NEP was found for an integration time between 0.5s and 1s.

The same result was found for all 6 modules of FM HS Sevenpack 1c, which is plotted in Fig. 45.

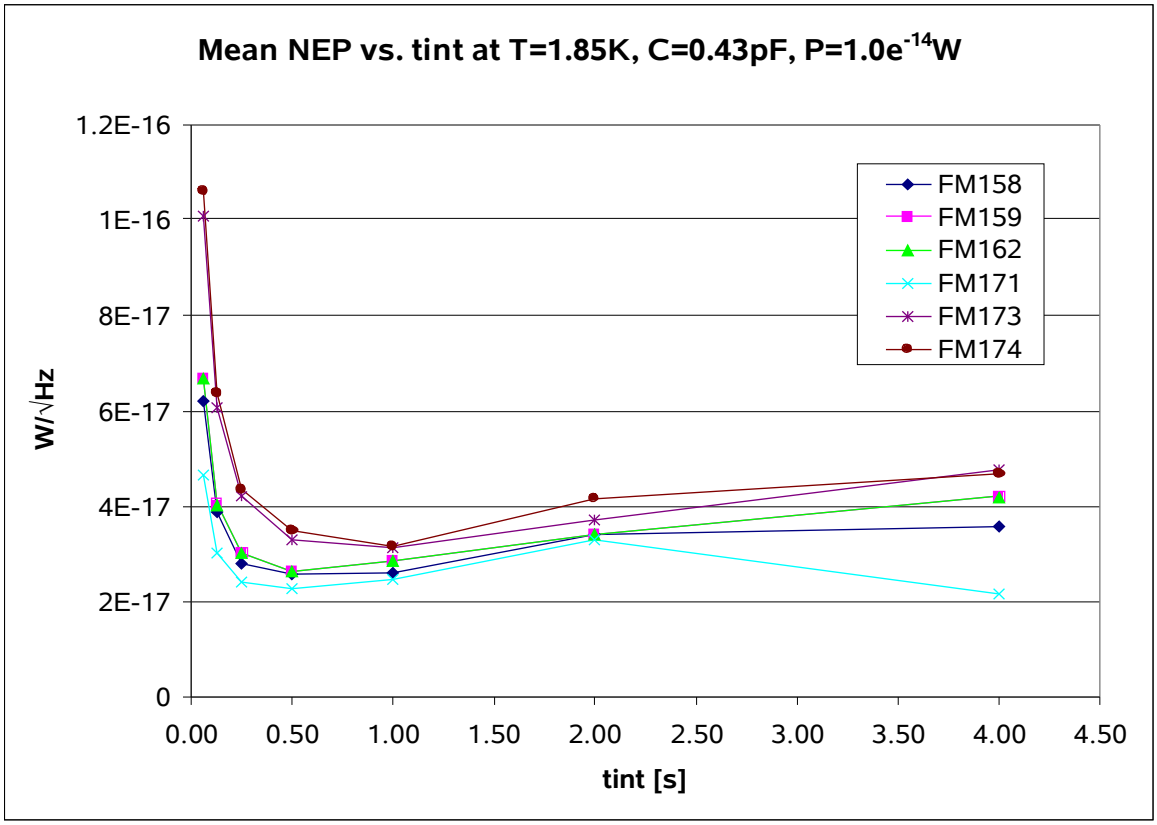

Fig. 45: NEP versus integration time of FM HS Sevenpack 1c

5.6 Module Selection for the High Stress Array

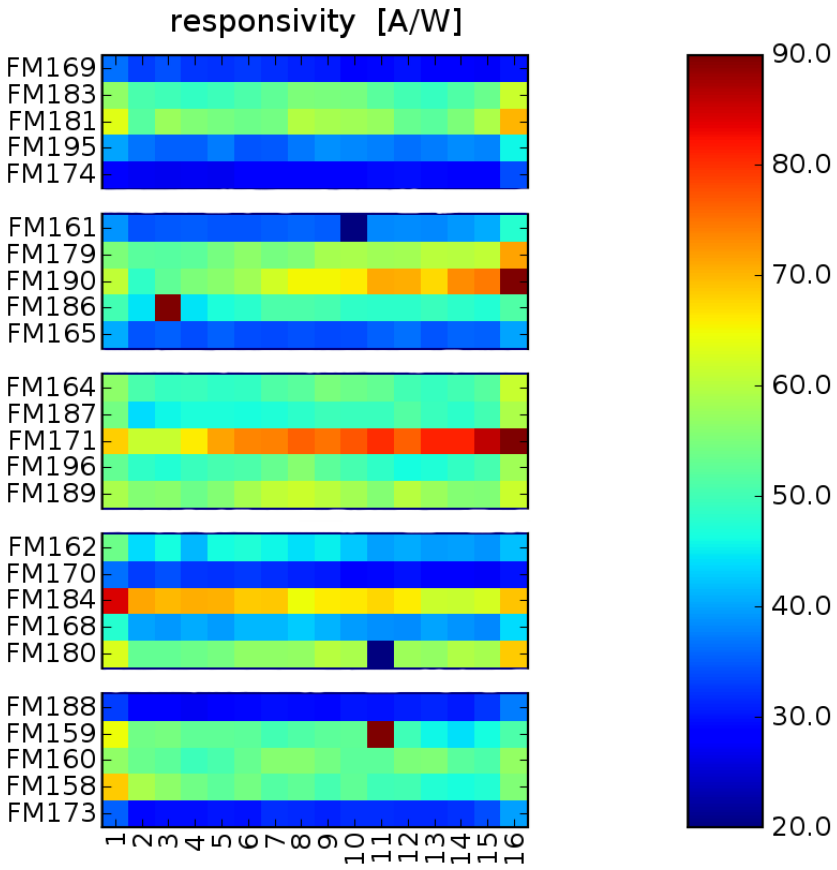

Fig. 46: Responsivity of the 25 selected modules of the low stress array (bias=70mV, T=1.85K)

6 Conclusion

Based on the presented test results, 25 modules out of 31 were selected for the assembly of the FM "Red Array". The criterion for the selection was the measured responsivity. Altogether, the following results were found:

- **Dark current:** Almost all assembled FM modules exceed the specified dark current of 50000e/s at 50mV bias, some modules by more than a factor of 2. Additional tests are foreseen to prove the dark conditions of the test set-up.
- **Responsivity:** The variation of the measured responsivity is roughly a factor of 3, between ~30 and ~90A/W. While the variation within the modules is acceptable, the difference between the modules is considerable. This strong variation makes it difficult to assemble a homogeneous array.
- **NEP:** For a flux of $4.2e^{-15}$W and the smallest integration capacity the calculated NEP was between 1 and $2e^{-17}$ W/√ Hz. The minimum NEP was found for a bias between 70mV and 80mV, depending on the responsivity of each module. For a flux of $2.4e^{-15}$W the lowest measured NEP was ~$8e^{-18}$ W/√ Hz.
- **Signal dependence from integration time:** The measurements with various integration times between 1/16s and 4s show a remarkable dependence of the signal slope on the integration time. While the calculated responsivity can change up to ~15%, the signal to noise ratio varies up to a factor of 10 (factor 6 expected, proportional to 1/√ t). The change of the NEP is module specific and lies between a factor 2 and 4. A minimum NEP was found between 0.5s and 1s integration time.